Space Weather

RESEARCH ARTICLE
10.1029/2022SW003121

Auroral Drivers of Large dB/dt During Geomagnetic Storms

Ying Zou[1], Caleb Dowell[1,2], Banafsheh Ferdousi[3], Larry R. Lyons[4], and Jiang Liu[4,5]

[1]Department of Space Science, University of Alabama in Huntsville, Huntsville, AL, USA, [2]Department of Mechanical Engineering, Colorado School of Mines, Golden, CO, USA, [3]Department of Physics and EOS Space Science Center, University of New Hampshire, Durham, NH, USA, [4]Department of Atmospheric and Oceanic Sciences, University of California, Los Angeles, CA, USA, [5]Department of Earth, Planetary and Space Sciences, University of California, Los Angeles, CA, USA

Key Points:

- We study disturbances responsible for geomagnetically induced currents by examining auroral drivers of large dB/dt during geomagnetic storms
- Large dB/dt is often driven by expanding auroral bulges, streamers, poleward boundary intensifications, omega bands, and pulsating auroras
- The onset, spatial variability, and duration of large dB/dt are well explained by those of the auroras

Correspondence to:

Y. Zou,
yz0025@uah.edu

Citation:

Zou, Y., Dowell, C., Ferdousi, B., Lyons, L. R., & Liu, J. (2022). Auroral drivers of large dB/dt during geomagnetic storms. *Space Weather*, *20*, e2022SW003121. https://doi.org/10.1029/2022SW003121

Received 11 APR 2022
Accepted 17 AUG 2022

Author Contributions:

Conceptualization: Banafsheh Ferdousi, Larry R. Lyons, Jiang Liu
Formal analysis: Caleb Dowell
Investigation: Caleb Dowell
Methodology: Banafsheh Ferdousi
Writing – review & editing: Caleb Dowell, Banafsheh Ferdousi, Larry R. Lyons, Jiang Liu

Abstract Forecasting geomagnetically induced currents (GICs) remains a difficult challenge, and open questions hindering our understanding include when and where GICs become large and what magnetospheric and ionospheric processes are responsible. This paper addresses these questions by determining the auroral drivers of large dB/dt (>100 nT/min, a proxy for GICs) on the ground during geomagnetic storms. We study auroras because, although the current system driving dB/dt is at times challenging to reconstruct, the accompanying auroras are routinely measured in high resolution. For various types of auroras, our community has already acquired a deep understanding of the driving mechanisms and spatiotemporal characteristics. Using coordinated observations from THEMIS and Geophysical Institute Magnetometer Array magnetometers and THEMIS all-sky imagers, we statistically examine large dB/dt intervals during storms from 2015 to 2016. A variety of auroral drivers have been identified, including poleward expanding auroral bulges, auroral streamers, poleward boundary intensifications, omega bands, pulsating auroras, etc. The onset, spatial variability, and duration of large dB/dt are well explained by those of the auroras. For example, poleward expanding auroral bulges drive large dB/dt that spread progressively poleward, and periodic injections of streamers drive large dB/dt that occur in periodic bursts. By referring to the magnetospheric source of the auroras, the magnetospheric source of large dB/dt can be inferred, whether it be dipolarization of the tail magnetic field, bursty bulk flows, instability, or wave-particle interaction. Our results suggest that auroras can exert significant leverage on GIC research and forecast.

Plain Language Summary One of the most significant space weather effects is geomagnetically induced currents (GICs), yet knowledge of when and where GICs become large and what magnetospheric and ionospheric processes are responsible is limited. One promising way to create a breakthrough is to establish the relation between GICs and auroras. This is because the high-latitude current system driving GICs is accompanied by auroras, and auroras are routinely measured in high resolution. For various types of auroras, our community has already acquired a deep understanding of the driving mechanisms and spatiotemporal characteristics. This paper therefore examines the auroral drivers of large dB/dt (>100 nT/min, a proxy for GICs) on the ground during geomagnetic storms. A variety of auroral drivers have been identified, including poleward expanding auroral bulges, auroral streamers, poleward boundary intensifications, omega bands, pulsating auroras, etc. The spatial and temporal characteristics of large dB/dt are similar to those of the auroras, and the similarity has important applications because the challenge in determining the spatial variability, onset, and duration of large dB/dt can be alleviated by referring to auroras. The magnetospheric source of dB/dt can also be inferred. Our results therefore suggest that auroras can exert significant leverage on GIC research and forecast.

1. Introduction

Society is becoming increasingly vulnerable to space weather disturbances, and one of the most significant space weather effects is geomagnetically induced currents (GICs) that flow in electric power grids, pipelines, railways, and communication cables. The severity of a GIC event for an electric utility depends on two sets of factors. One set is the surface horizontal geoelectric field, which is related to the rate-of-change of the horizontal component of the geomagnetic field (dB/dt) that is often measured in nanotesla per minute (nT/min) or nanotesla per second (nT/s). The other set is the type of equipment used and the way in which it is deployed (including the orientation of the transmission lines, their length, the electrical DC resistance of the transmission conductors and transformer

windings, the transformer type and mode of connection; and the method of station grounding and resistance (Molinski, 2002)). We mainly focus on dB/dt in the current paper because large dB/dt can develop and propagate rapidly, simultaneously expose large geographic areas, and have been acknowledged as an important indicator for a potential GIC hazard. It is also readily observable with useful spatial coverage.

Extreme dB/dt values exceeding 2,000 nT/min have been observed in association with intense GICs, yet relatively low levels of disturbance, such as at 100 nT/min, are sufficient to cause adverse socioeconomic impacts (Kappenman, 2006). For example, the Hydro-Quebec blackout during the March 1989 storm was triggered by dB/dt with a peak intensity of 479 nT/min (~8 nT/s) (Fiori et al., 2014; Kappenman et al., 2000). The regional power grid blackout in Malmo, Sweden during the 2003 Halloween storm was associated with dB/dt with a peak intensity of 308 nT/min (~5 nT/s) (Kappenman, 2005). Disturbances of ~60 nT/min (1 nT/s) have driven GICs of several amperes or larger in the Finnish high-voltage power system (Viljanen, 1997), and GICs of this intensity are alarming as they can put certain types of transformers out of the linear mode (Vakhnina et al., 2015). Two commonly used thresholds for high-risk dB/dt are 1.5 nT/s (Pulkkinen et al., 2011, 2013) and 5 nT/s (Molinski, 2002; Molinski et al., 2000). Lower thresholds, such as 60 nT/min (1 nT/s), have also been used (for example, Viljanen & Tanskanen, 2011; Viljanen et al., 2001).

Despite that GICs have been studied for decades, outstanding open questions remain concerning where and when they occur and their physical driver. Climatically, the rate-of-change of the north-south component of the geomagnetic field (dB_N/dt) maximizes in the pre-midnight and prenoon sectors (Juusola et al., 2015; Weigel et al., 2002, 2003), the maxima being located at the night- and dayside ends of the average westward electrojet, respectively. The pre-midnight maximum is most intense during southward IMF orientation, and the morning maximum is most intense during fast solar wind speed and radial IMF orientation (Juusola et al., 2015). A similar double-peak pattern is also found when studying the occurrence of large dB/dt only, large being defined as >60 nT/min in Viljanen et al. (2001) and Viljanen and Tanskanen (2011), >360 nT/min in McCuen et al. (2021), and >500 nT/min in Schillings et al. (2021). The direction of these large dB/dt vectors is primarily north-south in the pre-midnight sector, whereas it becomes much more scattered and even prefers an east-west orientation in the morning sector. The pre-midnight dB/dt is possibly due to sudden intensification of the west- or eastward electrojet in association with substorms, and the morning dB/dt due to localized and rapidly changing current structures generated by ULF pulsations associated with the Kelvin-Helmholtz instability (Weigel et al., 2003), or with the foreshock and quasi-parallel region of the bow shock (Juusola et al., 2015). However, it is noteworthy to mention that the above climatical morphology may not represent dB/dt activity in individual events. The exact location and time of large dB/dt differ from event to event, and the number of large dB/dt spikes is not necessarily correlated with the intensity of a storm defined by planetary indices such as Dst or AE (Schillings et al., 2021).

What is not reflected in the climatical morphology is the localized nature of GICs and associated geoelectric field and dB/dt. Pulkkinen et al. (2015) reported that the geoelectric field at one site could be five times larger than at nearby sites at only about 240 and 280 km distance, manifesting as extremely localized peaks. Ngwira et al. (2015, 2018) found that these extremes can occur over a wide range of latitudes (50°–85° MLAT) and local times, and that some of them follow the poleward edge of the poleward expanding aurora. Similarly, Engebretson, Pilipenko, et al. (2019) reported that the statistical distribution of large dB/dt shows a ~275 km effective radius, beyond which the dB/dt amplitude drops in half. Engebretson et al. (2020) further characterized the half-amplitude falloff distances separately in the latitudinal and longitudinal directions, the former being 106–204 km, and latter being 262–446 km. Dimitrakoudis et al. (2022) determined the vector correlation lengths of dB/dt and found that in the auroral oval a separation of ~200 km is needed to capture the spatial variability of dB/dt. However, equatorward of the auroral oval, the correlation remains comparatively high for distances >400 km. Dimmock et al. (2020) revealed that the regional (~500 km) dB/dt variability tends to increase with geomagnetic indices, the southward component of the IMF, and the solar wind speed, although these dependencies have considerable data scatter.

The localized nature of dB/dt remains a challenge in GIC research and forecast, and as suggested by Ngwira et al. (2018), the localization most likely results from the mapping of certain magnetosphere disturbances to the ionosphere. Although preliminary, progress has been made in specifying those magnetosphere disturbances. For example, Engebretson, Steinmetz, et al. (2019) studied intervals of nighttime magnetic perturbations and found that they are associated with the substorm poleward expanding auroral bulge and its westward traveling surge. The expanding auroral bulge is the ionospheric segment of the substorm current wedge (SCW). It maps

Table 1
Geographic and Altitude Adjusted Corrected Geomagnetic Coordinates Locations of the Geophysical Institute Magnetometer Array Magnetometers Utilized in the Study

Ground magnetometer	GLAT (°)	GLON (°)	MLAT (°)	MLON (°)
INUV	68.4	−133.8	71.6	−83.7
KAKO	70.1	−143.7	71.2	−93.2
FYKN	66.6	−145.2	67.4	−91.6
EAGL	64.8	−141.2	66.3	−86.7
POKR	65.1	−147.4	65.5	−92.5
CIGO	64.9	−147.9	65.2	−92.8
KIAN	67.0	−160.4	65.4	−104.5
WHIT	61.0	−135.2	63.6	−78.8
TRAP	62.2	−150.4	62.0	−93.5
MCGR	63.0	−155.6	61.9	−98.3

to a tailward and azimuthal expansion of the dipolarized region in the inner magnetosphere that is formed in association with flow bursts transporting magnetic flux from the reconnection site to the near-Earth region (Kepko et al., 2015 and references therein). Similarly, Weygand (2021) discovered that dB/dt suddenly increases at the auroral onset time and expands westward, eastward, and poleward throughout the substorm expansion phase. Then dB/dt gradually returns to pre-substorm levels during the recovery phase, and the peak shifts westward and poleward. On the other hand, Apatenkov et al. (2020) found that the largest ever recorded GICs at the northernmost Vykhodnoy transformer were associated with wave-like auroral structures with shapes resembling the Greek letter Ω, that is, omega bands (Akasofu & Kimball, 1964). Engebretson et al. (2020) also reported that omega bands are responsible for driving hemispherically conjugate magnetic perturbations that drift eastward at ∼1.3 km/s in the post-midnight sector. Often occurring in the morning sector of the auroral oval, omega bands drift eastward at speeds of 0.4–2 km/s (Mravlag et al., 1991; Opgenoorth et al., 1983; Yamamoto et al., 1993). Although the exact generation mechanism is under debate (see references in Liu et al. (2018)), the most popular mechanisms are the Kelvin-Helmholtz instability driven by the flow shear between flows in the plasma sheet and the low-latitude boundary layer (Connors & Rostoker, 1993; Rostoker & Samson, 1984), and the shear associated with high-speed earthward flows injected into the inner magnetosphere (Henderson, 2012; Partamies et al., 2017; Weygand et al., 2015) or dawnward flows resulting from the diversion of the earthward flows (Liu et al., 2018, 2020; Weygand et al., 2022).

However, the expanding auroral bulge and omega band are not the only types of magnetotail disturbances, nor are they the only auroral forms capable of driving large dB/dt. Weygand (2021) found that a sudden brightening and distortion of auroral arcs can produce large rapid changes in the magnetic field of hundreds of nT. The current paper aims to systematically investigate the nighttime auroral drivers of large dB/dt. We study auroras because, although the magnetosphere-ionosphere current system that drives large dB/dt is challenging to reconstruct, the accompanying auroras are routinely measured in high resolution and over wide regions. Furthermore, for various types of auroras, our community has already acquired a fairly deep understanding of the spatiotemporal characteristics and the driving mechanisms. As seen in Sections 3 and 4, our results show that large dB/dt can occur in close association with poleward expanding auroral bulges (including the westward traveling surges), auroral streamers, poleward boundary intensifications, omega bands, and pulsating auroras. By establishing the relation between auroras and large dB/dt, the fruitful progress in auroral research and forecast can be applied to the aforementioned outstanding challenges for understanding where and when large dB/dt occurs and its physical driver, and can hence be used to improve the accuracy and timeliness of GIC forecasting. Note that although we refer to auroras as drivers of large dB/dt, it is the aurora-associated electric currents which originate from the magnetosphere that physically drive dB/dt.

It is worth mentioning that although the drivers of localized GICs or large dB/dt have not been thoroughly identified, the geomagnetic conditions that favor their occurrence have been extensively documented. They have been shown to occur during the arrival of interplanetary shocks at the magnetosphere (for example, Belakhovsky et al., 2017; Fiori et al., 2014; Oliveira et al., 2018; Zhang et al., 2015), storms (for example, Carter et al., 2016; Dimmock et al., 2019; Kappenman, 2005; Kozyreva et al., 2018; Pulkkinen et al., 2003, 2005), substorms (for example, Engebretson, Pilipenko, et al., 2019; Engebretson, Steinmetz, et al., 2019b; Freeman et al., 2019; Viljanen et al., 2006; Weygand, 2021), and geomagnetic pulsations (Belakhovsky et al., 2019; Heyns et al., 2021; Yagova et al., 2021). The geomagnetic condition of our interest is storms, and the investigation of the auroral drivers during other geomagnetic conditions is deferred to future studies.

2. Data Set

The coordinated measurements of auroras and dB/dt are obtained from THEMIS All-Sky Imagers (ASIs), THEMIS Ground Magnetometers (GMAGs), and Geophysical Institute Magnetometer Array (GIMA). Tables 1 and 2 list the magnetometer and ASI stations utilized in the current study and their geographic and geomagnetic

Table 2
Geographic and Altitude Adjusted Corrected Geomagnetic Coordinates Locations of the THEMIS All-Sky Imagers Utilized in the Study

THEMIS ASI	GLAT (°)	GLON (°)	MLAT (°)	MLON (°)
INUV	68.4	−133.8	71.3	−82.2
FYKN	66.6	−145.2	67.4	−91.6
KIAN	67.0	−160.4	65.4	−104.5
WHIT	61.0	−135.2	63.6	−78.8
GAKO	62.2	−150.4	62.0	−93.5
MCGR	63.0	−155.6	61.9	−98.3

locations. We primarily focus on the Alaskan region due to the dense magnetometer coverage at a resolution up to a few hundred km between latitudes 60° and 72° MLAT, which permits identification of spatial variability of dB/dt in the auroral zone. The physical relation between large dB/dt and auroral drivers revealed from the Alaskan sector should have wide applicability to the other parts of the auroral oval. The Alaskan magnetometers have a temporal resolution of 0.5 and 1 s, capable of capturing small temporal-scale features and accurately measuring dB/dt. For consistency, we interpolate all magnetometer data linearly to 1 s. Because magneotometers across the world operate at various temporal resolutions, and dB/dt can be sensitive to the temporal resolution, we also downsample the 1 s data to 1 min and examine the extent to which dB/dt is affected. For instance, the magnetometer data at SuperMAG are often of 1 min cadence (Gjerloev, 2012), and our down-sampling would reveal the extent to which the 1 min data can capture the large dB/dt driven by auroras. We use THEMIS ASIs mostly qualitatively to identify various auroral forms, because the ASIs do not measure auroral brightness in absolute units, such as Rayleighs, and were not designed for quantitative interpretation (Mende et al., 2009). Nevertheless, the ASI white light counts still provide useful information. For precipitating electrons with an energy >3 keV, the counts are closely proportional to the total precipitated energy (Mende et al., 2009), and initial success have been achieved in converting the counts to red, green, and blue intensities in absolute units so as to estimate the precipitating energy flux and average energy (Gabrielse et al., 2021).

When computing dB/dt, we use the total horizontal component of the magnetic field, which is obtained as $B = \sqrt{B_n^2 + B_e^2}$, where B_n and B_e are the measured northward and eastward components of the geomagnetic field, respectively. *L*arge dB/dt events are defined as 10 min intervals where the upper quartile of dB/dt exceeds 100 nT/min at one or more magnetometers. The purpose of using the upper quartile is to identify high-risk dB/dt that occur for a significant fraction of time (25% of the 10 min interval). The peak value, on the other hand, is also important and is computed as the 98 percentile to minimize chances of selecting peculiar peaks that could potentially be due to instrument or random errors. As seen below, the peak value has exceeded 300 nT/min in many cases, occasionally even 1,000 nT/min.

Large dB/dt events are selected automatically, where the program extracts and computes the upper quartile of a 10 min sliding window that slides at a 5 min time step. For each selected interval, we visually inspect auroral observations to search for auroras that coincide with and have similar spatial and temporal characteristics similar to, dB/dt. We found that most of the events are driven by one of the following auroras: poleward expanding auroral bulges, auroral streamers, poleward boundary intensifications, omega bands, and pulsating auroras. Representative cases demonstrating the connection between dB/dt and these auroras are presented below.

3. Case Studies

3.1. Poleward Expanding Auroral Bulge

Figure 1 exemplifies events when large dB/dt (upper quartile >100 nT/min as defined above) is driven by poleward expanding auroral bulges. This category also includes westward traveling surges because the surges are the western edge of the bulges. Figures 1a and 1b show the SYM-H and AE indices of the storm on 17 March 2015. The interval of interest, as highlighted in yellow, occurred during the recovery phase of the storm and during a transition from the growth to the expansion phase of a substorm. Figures 1c–1f show representative 2D snapshots of the auroral activity and associated dB/dt in AACGM coordinates. Here auroras are color-coded in gray scale, and dB/dt is represented by the open red circles with a center (marked as the plus sign) at the magnetometer station and a radius proportional to the dB/dt magnitude (a legend in the upper left corner of Figure 1c). The names of the magnetometer stations are labeled in yellow. Figures 1g–1n present the time evolution of the auroras and the dB/dt's as time series plots, and the measurements from various stations are organized from highest to lowest latitudes.

Initially, the auroral oval was quiet and expanded gradually equatorward, and the oval was dominated by an extended east-west auroral arc (Figures 1c and 1h). Variations in the geomagnetic field were small, with dB/dt

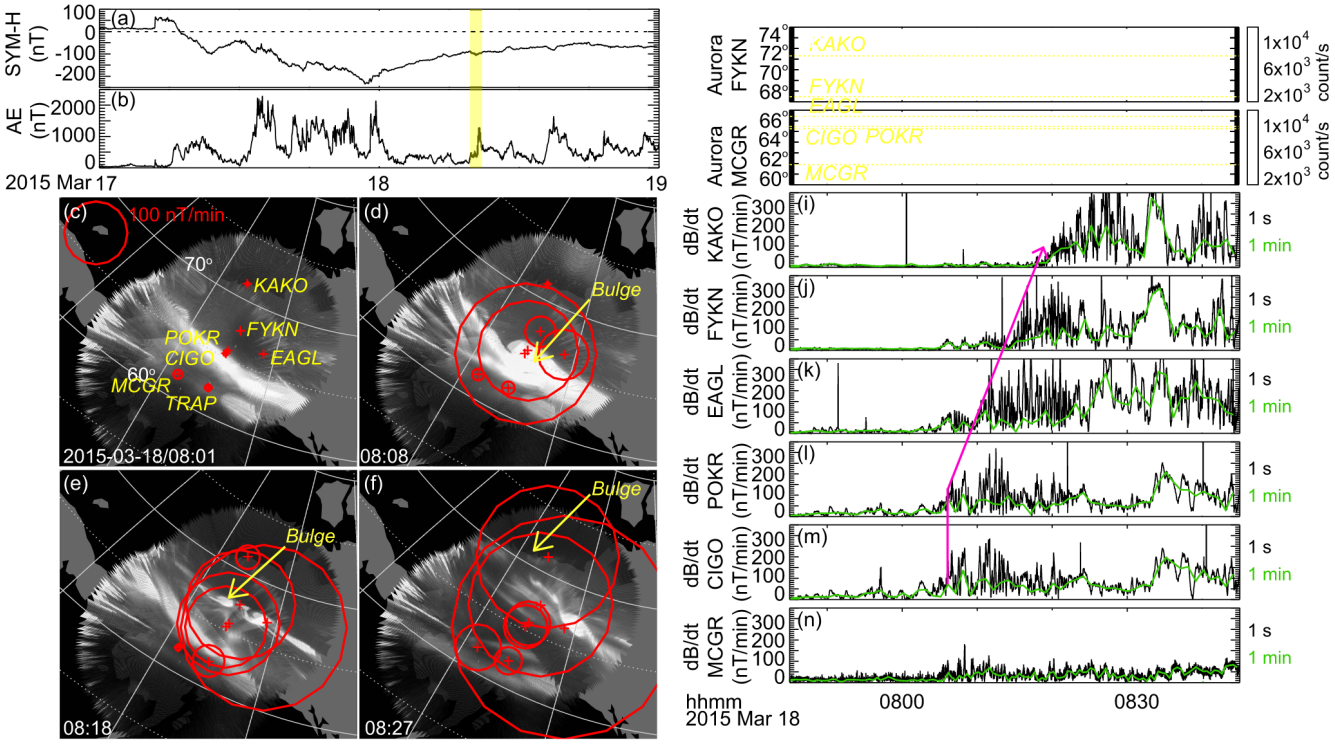

Figure 1. (a–b) SYM-H and AE indices taken from OMNI. The yellow shaded region highlights the interval of our interest. (c–f) Snapshots showing auroras (gray scale) and dB/dt (red open circles) in the Altitude adjusted corrected geomagnetic coordinates (AACGM). The size of the circle representing 100 nT/min is illustrated in the top left corner of Figure 1c. (g–h) Time series plots of auroras as measured by the FYKN and MCGR All-Sky Imagers (ASI). (i–n) Time series plots of dB/dt as measured by KAKO, FYKN, EAGL, POKR, CIGO, and MCGR magnetometers. The magnetometers are organized from high to low latitudes, and their geomagnetic latitudes are illustrated in Figures 1g and 1h as the horizontal yellow dotted lines. The black curve represents dB/dt computed at 1 s cadence data, and the green curve represents 1 min cadence data. The magenta arrow illustrates the poleward spreading of large dB/dt.

being low tens of nT (Figures 1c, 1i–1n). After 0805 UT, the east-west auroral arc intensified, deformed, and expanded poleward and azimuthally, forming a bulge (Figures 1d–1f, 1g and 1h). Close to the break-up arc, dB/dt at POKR and CIGO substantially enhanced, reaching a peak value of 228 nT/min at POKR, and 250 nT/min at CIGO, whereas poleward or equatorward of the arc, dB/dt remained small (Figures 1d, 1i–1n). The dB/dt enhancement then spread poleward with time together with the bulge, passing EAGL, then FYKN, and finally KAKO, where the peak value reached 356, 319, 468 nT/min, respectively. By down-sampling the magnetometer data to 1 min (green curve), although the peak magnitude of dB/dt decreased by several times, the occurrence of the enhancement in association with the auroral bulge is still discernible. The bulge began to retreat sometime between 0830 and 0840 UT, yet dB/dt remained elevated due to other ongoing auroral activities, which in the current case consists of auroral streamers.

This event demonstrates that the onset, localization, and duration of large dB/dt are all consistent with those of the poleward expanding auroral bulge. This is expected because the dynamic growth of the auroral bulge implies that the associated upward field aligned currents (FACs) and horizontal ionospheric currents were varying rapidly. On the other hand, auroras that are steady or evolve slowly, such as the east-west auroral arc prior to the onset of the expansion, are not effective in driving large dB/dt.

3.2. Auroral Streamer

Streamers, also named as north-south segments (Montbriand, 1971), equatorward-diving arcs (Henderson et al., 1994), north-south auroral forms (Henderson et al., 1994; Nakamura et al., 1993), and auroral fingers (Liu & Rostoker, 1993; Rostoker et al., 1987), are structures that originate from intense, transient auroral disturbances along the poleward boundary of the nightside auroral oval (i.e., poleward boundary intensifications, PBIs) and then propagate equatorward. They are auroral manifestations of earthward-moving plasma-bubble-produced flow

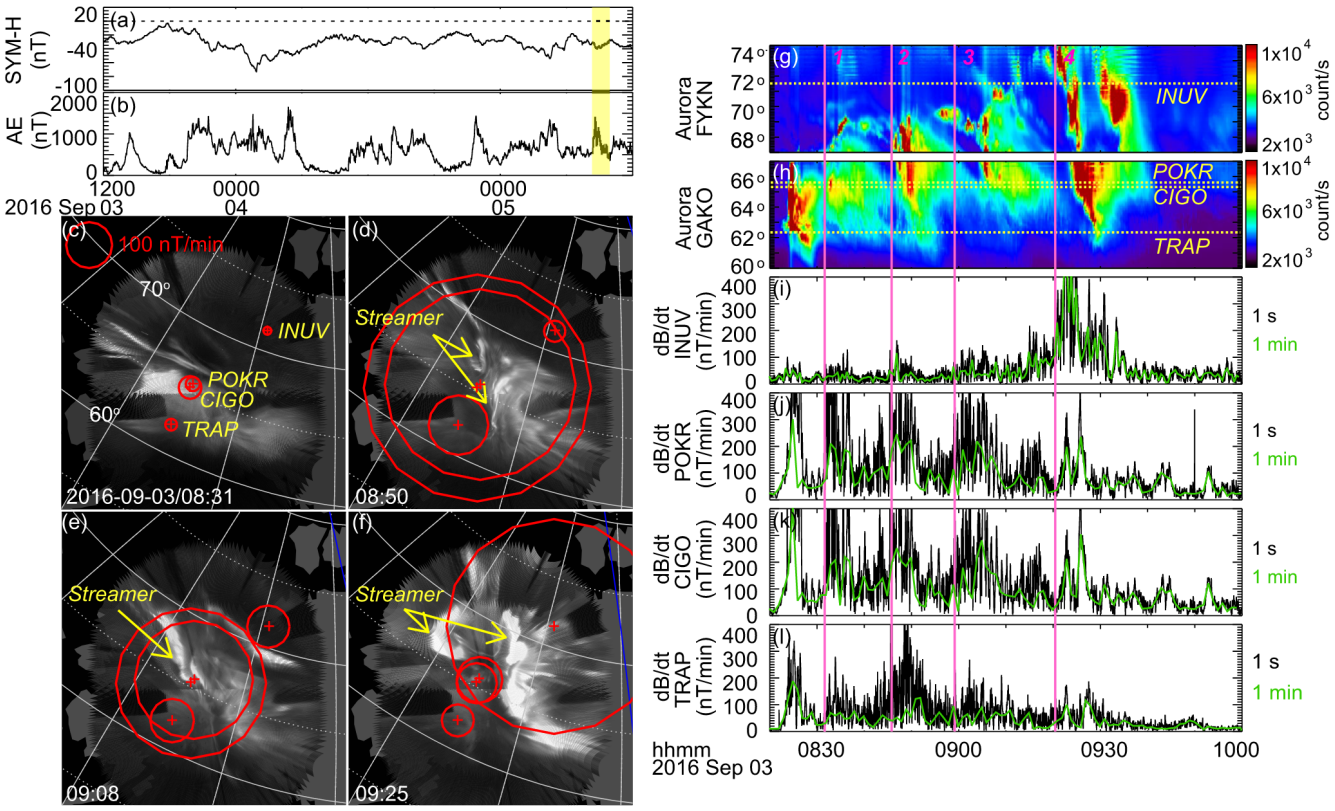

Figure 2. Similar to Figure 1 but showing dB/dt associated with auroral streamers on 3 September 2016. The dark blue line in Figures 2e and 2f mark the magnetic midnight. The four vertical magenta lines (labeled as 1–4) in Figures 2g–2l mark the four episodes of streamer activity.

bursts and hence represent effective transport of mass, energy, and magnetic flux from the tail reconnection site to the near-Earth region (Ferdousi et al., 2021; Lyons et al., 1999; Nakamura et al., 2001; Sergeev et al., 2000). They occur under all geomagnetic conditions, but the bright ones tend to occur during the substorm expansion and recovery phases.

Figure 2 presents an example of when large dB/dt was driven by streamers. This event occurred during the recovery phase of a multiple-dip storm that had the largest dip on 2 September 2016. It was also associated with a substorm, and a large fraction of the interval occurred during the substorm recovery phase (Figure 2b). Unlike the substorm expansion phase, when the bulge is comprised of a multitude of intense active auroral forms, making it challenging to isolate the effect of each form on dB/dt, auroral activity during the recovery phase can be dominated by one or two auroral forms only. For the event under analysis, the auroral activity over the Alaska region is dominated by a series of streamers. These streamers emerged quasi-periodically and can be grouped into four episodes as labeled in Figure 2g. The first episode (starting at ~0832 UT) originated from ~69° MLAT and propagated equatorward to 61°. The magnetometers located within this latitude range, TRAP, CIGO, and POKR, showed large dB/dt, whereas the INUV station located poleward was only marginally affected. Among TRAP, CIGO, and POKR magnetometers, the dB/dt at the most equatorward TRAP station was smaller than the other two (its peak magnitude being 216 nT/min vs. 592 and 571 nT/min), likely because the streamers had faded by the time they reached TRAP. The occurrence and spatial variability of dB/dt are also seen in the down-sampled 1 min data.

The second episode of streamers (starting at ~0846 UT) was similar to the first one except that it penetrated to a lower latitude, below ~61° MLAT. Consistent with the deeper penetration, dB/dt at TRAP intensified, with the peak reaching 414 nT/min. The third episode (starting at ~0859 UT) spanned a similar latitude range as the first episode, and so did the large dB/dt activity. In Figures 2j and 2k, the onset of the large dB/dt seemed to precede the streamers by a few minutes, and this was possibly because the streamers in this episode were initially oriented nearly east-west before rotating north-south (Figure 2e). For an east-west oriented and equatorward drifting arc

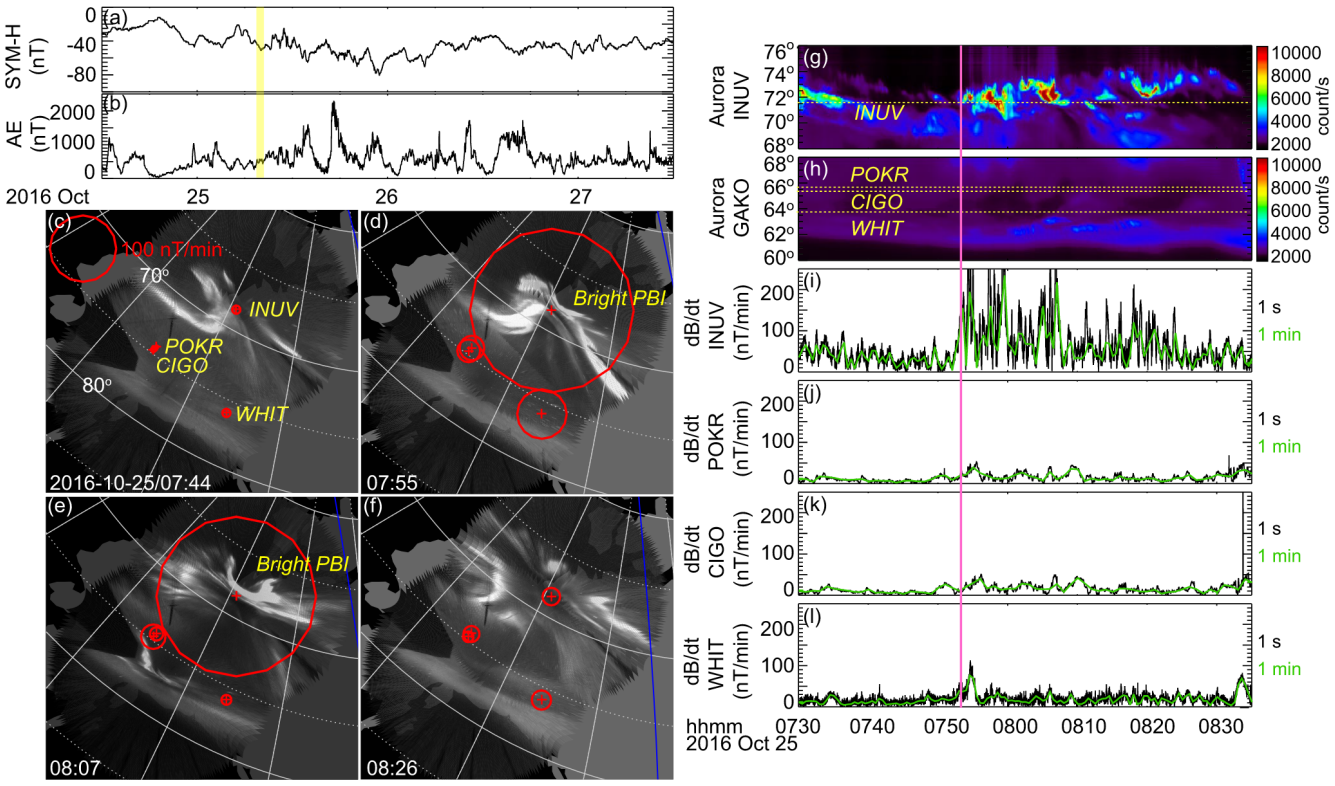

Figure 3. Similar to Figure 1 but showing dB/dt associated with poleward boundary intensifications (PBIs) on 25 October 2016. The vertical magenta line in Figures 3g–3l marks the onset of intensified PBI activity.

located in the pre-midnight sector, the horizontal ionospheric currents (both Pedersen and Hall) associated with the arc are often concentrated equatorward of the upward FACs (Aikio et al., 2002) and are therefore capable of affecting the magnetic field at POKR and CIGO before the arrival of the optical signature.

The last episode of the streamers (starting at ~0920 UT) originated from >74° MLAT beyond the ASI FOV, and the previously quiet INUV station now captured large dB/dt. In fact, the peak of dB/dt reached 831 nT/min. The large dB/dt then returned to small values as the streamer activity ceased. Therefore, similar to the first event, the onset, localization, and duration of large dB/dt are consistent with those of auroras, indicating an intimate connection between large dB/dt and streamers.

3.3. Poleward Boundary Intensification (PBI)

PBIs are intense and transient auroral intensifications at or near the nightside auroral poleward boundary (Lyons et al., 1999), and at times extend equatorward to lower latitudes inside the auroral oval (Zesta et al., 2002, 2006). Equatorward extending ones form auroral streamers, and non-equatorward extending ones appear as a series of multiple bead-like intensifications. PBIs have been interpreted as the auroral signature of magnetotail reconnection based on the observational facts that they are closely correlated with flow bursts in the tail plasma sheet (Lyons et al., 1999; Zesta et al., 2002, 2006), and that they form in association with a local thickening of the plasma sheet via the injection of new magnetospheric plasma, likely as the result of a bursty, patchy reconnection process (Hull et al., 2010). PBIs tend to occur repetitively with a period of ~10 min and during all levels of geomagnetic activity (Lyons et al., 1998), though they are more frequent following the substorm expansion phase than during quiet times.

Figure 3 presents a case where large dB/dt was driven by PBIs. To separate from streamers, we focus on PBIs that do not extend significantly equatorward (<2° MLAT) as occurred for the event in Figure 3. The event occurred during the main phase of a geomagnetic storm and was not associated with substorm activity (Figures 3a and 3b). From the beginning of the interval of our interest until 0753 UT, the auroral poleward boundary located around

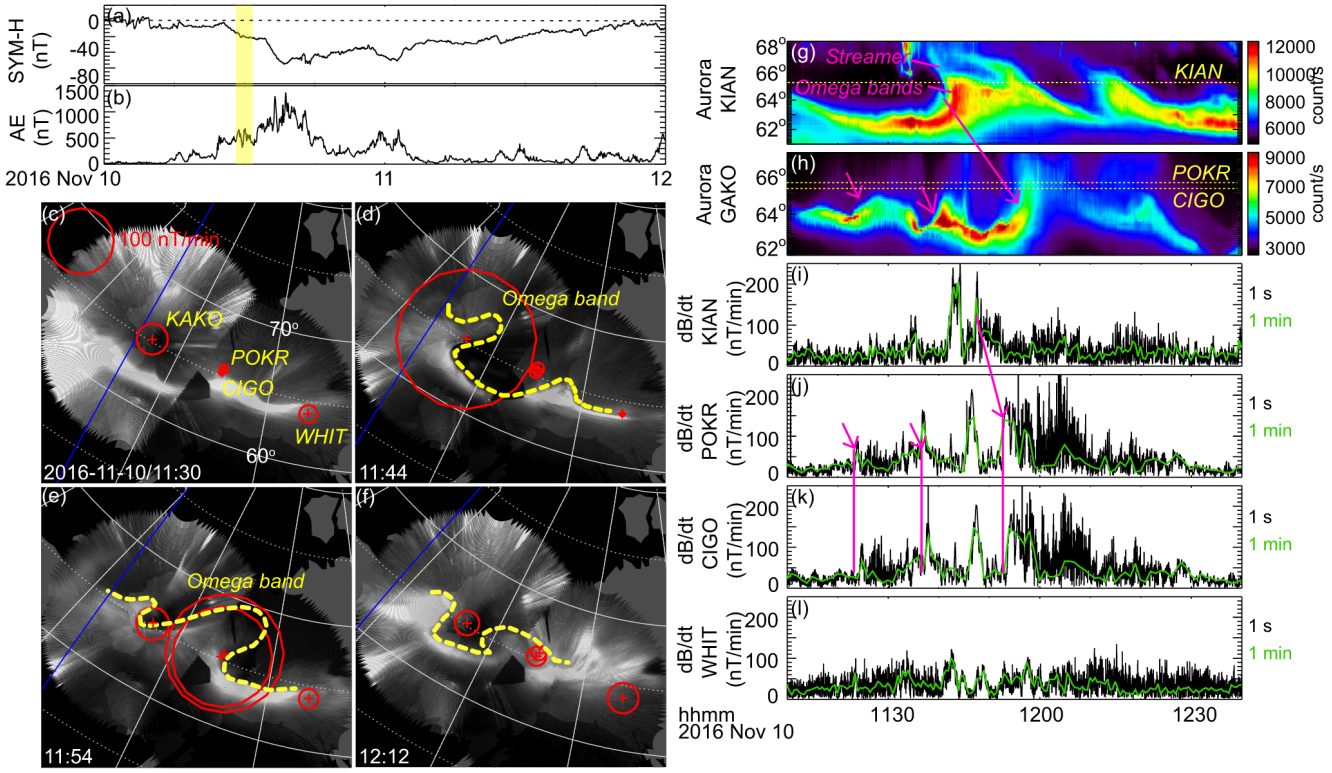

Figure 4. Similar to Figure 1 but showing dB/dt associated with omega bands on 10 November 2016. The yellow dashed curves in Figures 4d–4f outline the shape of omega bands. The magenta arrows in Figures 4g–4l represent the azimuthal propagation of omega bands from one station to the other.

72° MLAT showed relatively faint and quasi-steady PBIs whose intensity and shape evolved slowly over time (Figures 3c and 3g). The geomagnetic field at INUV showed variations mainly <100 nT/min, whereas the field at stations equatorward of the poleward boundary showed little perturbation (Figures 3i–3l). At 0753 UT, a new series of PBIs initiated. These PBIs were bright and were dynamically changing their shapes while drifting eastward (Figures 3d, 3e and 3g), and correspondingly, dB/dt at INUV became enhanced (Figures 3d, 3e and 3i). With a peak magnitude at 389 nT/min, the enhancement only occurred at INUV locally, where the poleward boundary was located, and stations located equatorward did not record large dB/dt. As the PBI activity subsided temporally after 0825 UT, dB/dt at INUV also reduced (Figures 3f and 3i). The occurrence and the localization of large dB/dt are also evident in the down-sampled 1-min data, similar to the previous two events.

3.4. Omega Band

As discussed in the introduction section, omega bands received their names due to the similarity of their shapes to the Greek letter Ω. They often occur in periodic sequences along the poleward boundaries of diffuse auroras toward the end of the substorm expansion and beginning of the recovery phase (Partamies et al., 2017). The bright and dark areas of the auroras are associated with east-west orientated pairs of upward and downward FACs that drift eastward together with the auroras (Opgenoorth et al., 1983).

Figure 4 shows a representative event where large dB/dt was driven by omega bands in the post-midnight sector (the first three events all took place in the pre-midnight sector). This event occurred during the main phase of the storm on 10 October 2016, and was associated with a quasi-steadily enhanced AE, which is a signature of steady magnetospheric convection (Kissinger et al., 2011; Figures 4a and 4b). Because of the eastward drifting motion of omega bands, we present magnetometers that are distributed along the east-west direction as opposed to the north-south direction in previous events. Before 1140 UT, the oval was dominated by an east-west aligned auroral arc with small bumps that drifted eastward toward the morning sector (Figure 4c). The bumps expanded gradually poleward as they drifted, reached a maximum around the longitudes of the POKR and CIGO magnetometers, and dissipated by the time reaching the WHIT magnetometer. Although the arc was overall located equatorward of

the KIAN, POKR, and CIGO magnetometers, modestly enhanced dB/dt (the peak being 84 nT/min at POKR and 104 nT/min at CIGO driven by the first bump, and being 153 nT/min at POKR and 150 nT/min at CIGO by the second bump) occurred when those small bumps passed the magnetometers (Figures 4i–4k).

At 1140 UT, a streamer extended into the FOV of the KIAN ASI toward the pre-existing east-west aligned arc, and the previously small bumps quickly expanded in size, acquiring a torch form (Figures 4g and 4h). A similar association between streamers and omega bands have been reported in Henderson (2012) and Weygand et al. (2015), where streamers are regarded as one prominent mechanism that contributes to the generation of omega bands (see introduction). The large torch is our main focus in this event, and as it drifted eastward, large dB/dt first initiated at the KIAN magnetometer at around 1147 UT, and then POKR and CIGO around 1153 UT (in Figures 4i–4k the large dB/dt spike centered at 1143 UT at KIAN and 1147 UT at POKR and CIGO are possibly driven by the streamer). The peak magnitude at these three stations was 179, 222, and 205 nT/min, respectively. Such large dB/dt did not occur at the easternmost station at WHIT because the torch had dissipated when reaching WHIT, and the dissipated structure was positioned poleward of the WHIT station (Figure 4l). In the absence of succeeding streamers impinging upon the pre-existing east-west aligned arc, omega bands following the large torch decreased substantially in sizes (Figures 4f–4h). Correspondingly, dB/dt returned to its initial variation level (Figures 4i–4l). The omega band-related large dB/dt is discernible in the down-sampled 1 min magnetometer data.

3.5. Pulsating Aurora

Pulsating auroras (PAs) are faint diffuse auroras consisted of east-west elongated or irregularly shaped patches that have a horizontal scale of 10–200 km and switch on and off with periods from a few to tens of seconds (Lessard, 2012; Royrvik & Davis, 1977; Yamamoto, 1988). They are predominantly observed after magnetic midnight, during the recovery phase of substorms, and at the equatorward boundary of the auroral oval. They are produced by precipitating energetic electrons originating from the modulation of magnetospheric electrons by wave-particle interactions (Fukizawa et al., 2018; Kasahara et al., 2018; Nishimura, Bortnik, et al., 2010, 2011). The candidate waves are lower-band chorus (LBC) (Kasahara et al., 2018; Nishimura, Bortnik, et al., 2010; Nishimura, Lyons, et al., 2010; Nishimura et al., 2011) and electrostatic electron cyclotron harmonic (ECH) waves (Fukizawa et al., 2018).

Although PAs are not produced by precipitating electrons accelerated by a field-aligned potential drop as discrete auroras do, they turn out to be effective in modulating the Earth's surface geomagnetic field and driving large dB/dt. Figure 5 presents one such event. This event occurred during the storm recovery phase and was also dominated by the recovery phase of a substorm (Figures 5a and 5b). When Alaska rotated to the midnight and post-midnight sectors, PA had already commenced and persisted for several hours. We focus on an interval toward the end of the PA activity to show dB/dt before and after the declination of the activity. During 1420 and 1500 UT, PAs can be identified as faint patches in the snapshots (Figures 5c–5e) and intermittent short vertical stripes in the keogram (Figures 5g and 5h). They were prominent at 64°–67° MLAT at the KIAN ASI and occupied a wider region at GAKO ASI with the poleward edge extending toward the edge of the GAKO FOV. Driven by PAs, dB/dt was large, with peak values being 228, 181, and 165 nT/min in the KIAN, POKR, and CIGO magnetometers (Figures 5i–5k). The large dB/dt exhibited a characteristic high-frequency fluctuating pattern that was not observed in the other auroral driver categories. In fact, the large dB/dt would not be captured if the magnetometer measurements were of low cadence, for example, of 1 min. The effectiveness of such high-frequency dB/dt fluctuations in driving GICs warrants further study, and earlier studies imply that they could be less effective than those with periods larger than 1 min. This is due to the skin depth effect in a conducting medium, where fluctuations of lower frequencies penetrate deeper into the Earth, increasing the size of the induction loop and subsequently induced currents, while higher frequencies can only penetrate to shallow depths, resulting in much smaller induction loops that are incapable of driving GICs (Oyedokun et al., 2020). Exceptions can occur at a significant geophysical strike (such as a coastline), where large conductive gradients usually arise at shallow depth. The large conductive gradients lead to large geoelectric fields and increase the possibility of GIC hazard. The WHIT magnetometer did not capture large dB/dt because it was located equatorward of the auroral oval (Figure 5l). The PA activity weakened after 1500 UT, and dB/dt also subsided (Figures 5f and 5g–l).

Similar PA-driven magnetic fluctuations have been reported (Campbell, 1970; Campbell & Rees, 1961; Heacock & Hunsucker, 1977). Because the time derivative of these magnetic variations can be expressed by a linear combination of the luminosity variations of auroral patches in various parts of the sky, Oguti et al. (1984) and

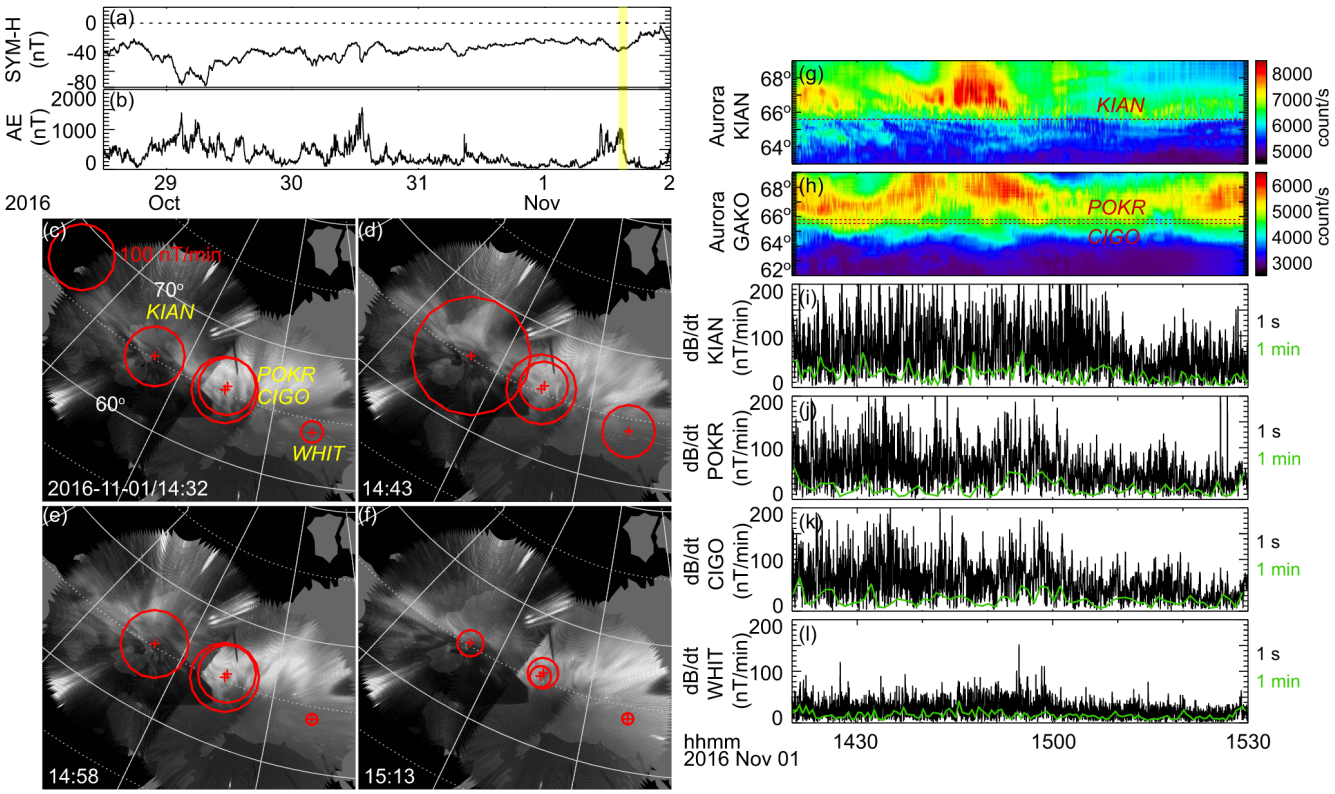

Figure 5. Similar to Figure 1 but showing dB/dt associated with pulsating auroras on 1 November 2016.

Oguti and Hayashi (1984) proposed that the magnetic variations are due to fluctuations of ionospheric currents resulting from conductivity fluctuations caused by the pulsating auroral precipitation. Their results are supported by Fujii et al. (1985), Sato et al. (2002, 2004), and Gillies et al. (2015), which detected FAC pairs in association with each pulsating patches with LEO spacecraft. Hosokawa and Ogawa (2010) further identified a Pedersen current closure in pulsating patches within the D region ionosphere. Therefore, albeit weak (a few μA/m^2, Gillies et al. (2015)), FACs associated with PAs can serve as an important source of large dB/dt.

4. Statistics

To understand how commonly large dB/dt is driven by various auroral drivers during storms, we perform a statistical survey of geomagnetic storms (minimum Dst < −50 nT) during 2015 and 2016. The auroral drivers during other geomagnetic conditions, such as substorms, are deferred to future study. Because THEMIS ASIs do not operate during summertime, we only survey January to April and September to December for each year. As mentioned earlier, large dB/dt events were selected as 10 min intervals where the upper quartile of dB/dt exceeds 100 nT/min at one or more magnetometers. We further require that clear auroral images were recorded by two or more ASIs surrounding the magnetometers to ensure spatially broad aurora coverage. The survey in total identified 641 intervals of large dB/dt with simultaneous auroral measurements.

For each dB/dt event, we determine whether it is driven by a poleward expanding auroral bulge, auroral streamer, poleward boundary intensification (PBI), omega band, pulsating aurora (PA), or something else. Poleward expanding auroral bulges, referred to as bulges below, are identified as the rapid expansion of auroras by >4° in MLAT from an arc located near the equatorward boundary of the oval. This category includes westward traveling surges because the surges are the western edge of the bulges. The bulge is comprised of a multitude of intense active auroral forms, including streamers and PBIs, and the effect of the bulge on dB/dt represents the collective effects of them all (except for PA, which occurs equatorward of the bulge).

On the other hand, the effect of individual auroral forms is assessed when the oval does not explosively expand but is, at a given local time, dominated by one or two auroral forms only. Such conditions generally correspond to the

Table 3
Geomagnetic Storms That are Associated With Large dB/dt and Clear Auroral Images

Date at minute Dst	Minute Dst
4 January 2015	−71
7 January 2015	−99
18 February 2015	−64
24 February 2015	−56
02 March 2015	−55
17 March 2015	−222
11 April 2015	−75
07 October 2015	−124
03 November 2015	−55
07 November 2015	−89
16 February 2016	−57
06 March 2016	−98
15 March 2016	−56
02 April 2016	−56
14 April 2016	−59
01 September 2016	−59
29 September 2016	−66
13 October 2016	−104
29 October 2016	−64
03 November 2016	−50
10 November 2016	−59

substorm recovery phase or during the time between substorm occurrence, and are identified by requiring that the oval in the THEMIS ASI data either has a quasi-steady width or is waning. The expansion phase, which lasts for about 30 min statistically (Gjerloev et al., 2007), is usually excluded. Streamers are identified as auroral arcs extending equatorward from the poleward boundary of the oval by >2° in MLAT, and PBIs as auroras along the poleward boundary without such equatorward extension. Omega bands are identified as auroral arcs that have bumps, torches, or tongues that drift eastward, and pulsating auroras as patches that switch on and off with periods from a few to tens of seconds.

Table 3 lists the storms that have intervals satisfying our event selection criteria, and Figure 6a presents the minimum Dst of these storms. The majority of the analyzed storms are modest in intensity, although there are two intense storms and one super storm. Figure 6b presents the local time distribution of the large dB/dt intervals. Most of the intervals occurred in the pre-midnight and midnight sectors. The dusk sector has the least number of events possibly because the occurrence rate of large dB/dt is lower than that in the nighttime sector (McCuen et al., 2021; Schillings et al., 2021; Viljanen & Tanskanen, 2011; Viljanen et al., 2001). Available auroral observations are also fewer because the proximity to the solar terminator means that the auroral observations are more subject to sunlight contamination than those in the nighttime sector. We do not have observations at the dawn sector because of the sunlight contamination.

Figure 7 shows how common large dB/dt is driven by various auroral drivers at the dusk, pre-midnight, midnight, and post-midnight sectors (Figures 7a–7d). At dusk, large dB/dt is driven by auroral bulges (58.0%), streamers (32.0%) and PBIs (10.0%). Note that the streamers and PBIs are selected from either substorm recovery phase or non-substorm time, implying that 42% of large dB/dt occur under conditions other than the expansion phase. In the pre-midnight sector, the dominant drivers are auroral bulges (33.0%) and streamers (43.6%), and the minor drivers now include PAs (6.2%) in addition to PBIs (6.6%). There are times when more than one type of auroral forms occur in proximity to the magnetometers that have recorded large dB/dt, and one example is the "PA + streamer" category in orange. The "other" category in magenta includes propagating diffusive patches and Harang aurora (Nishimura, Lyons, et al., 2010; *Zou* et al., 2012), ray-structured auroras (Størmer, 1955; Sandahl et al., 2008), etc. These auroral drivers occur much less repetitively than the five we identified and therefore are grouped into one category.

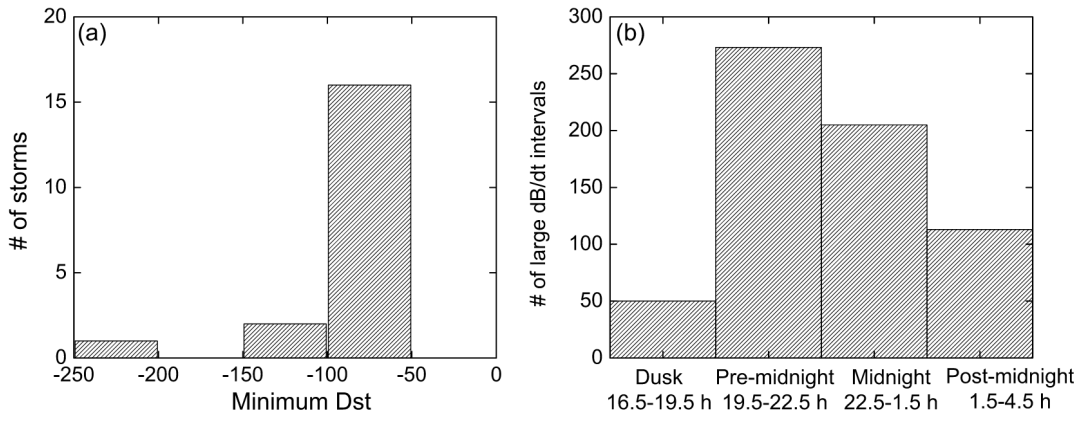

Figure 6. (a) Distribution of the minimum Dst of all the geomagnetic storms under analysis. (b) Magnetic local time distribution of the large dB/dt intervals under analysis. Here the magnetic midnight at Alaska is taken as 11:30 UT.

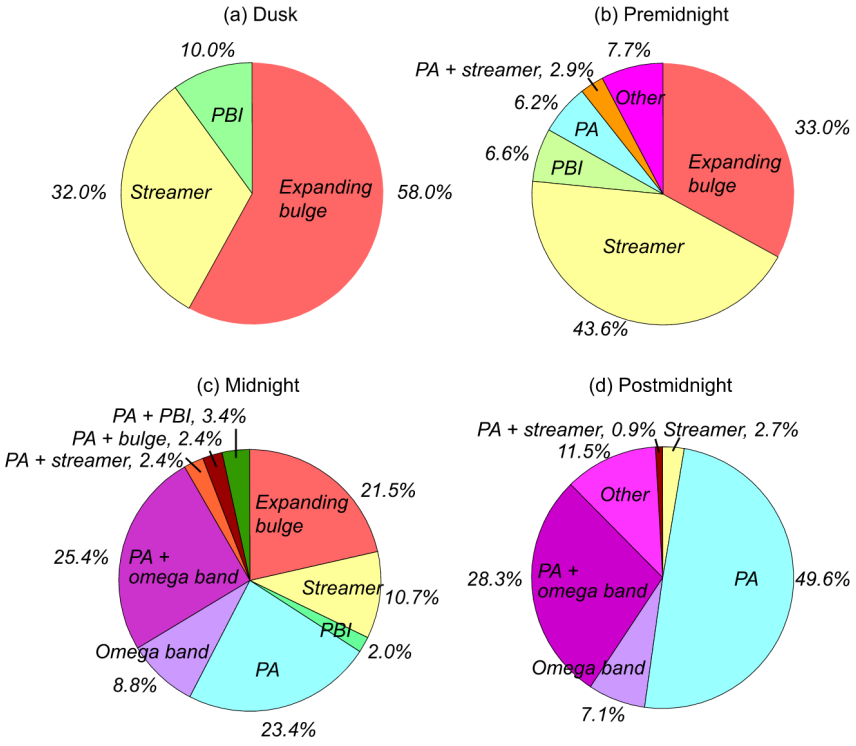

Figure 7. Pie chart showing the percentage of time of large dB/dt intervals being driven by various auroral drivers. Panels (a–d) represent large dB/dt intervals in the dusk, pre-midnight, midnight, and post-midnight sectors, respectively.

At midnight, dB/dt has diverse drivers. In addition to bulges (21.5%) and streamers (10.7%), PAs and omega bands play important roles, which is not surprising because they have been recognized as common auroral features in the midnight to morning sectors during geomagnetically active time. Compared with times when the oval is dominated by omega bands alone (as seen in Figure 4), it is more common for omega bands to occur together with PAs. When the latter happens, it becomes difficult to separate the effect of the two auroras because omega bands are often located immediately poleward of PAs, and we classify this situation as "PA + omega band." PAs have also been observed to occur simultaneously with streamers (PA + streamer category), PBIs (PA + PBI category), and bulges (PA + bulge category), but these categories are comparatively minor. Large dB/dt at the post-midnight sector is primarily driven by PAs and omega bands. The "other" category is primarily consisted of ray-structured auroras in the morning sector.

Figure 8 presents the magnitude of large dB/dt (based on 1 s data cadence) as a function of the AE index driven by different auroras. We examine the dependence on AE rather than Dst because of the limited variance range of Dst (most of the studied storms are modest in intensity). Each open circle presents the upper quartile of a 10 min large dB/dt interval, and similar to Figure 7, data are separated according to the local time sectors. Here we only focus on large dB/dt with a single auroral driver. Several features have been noticed. Firstly, dB/dt spans a larger range, and therefore can reach higher values, in the dusk and pre-midnight sectors than in the midnight and post-midnight sectors. For example, the upper quartile in the midnight and post-midnight sectors is predominately below 300 nT/min, but can reach 500 nT/min and above at earlier MLTs. This is probably related to the fact that the midnight and post-midnight sectors are dominated by omega bands and PAs (Figures 7c and 7d), and the FACs associated with these auroras are generally weaker than those associated with auroral bulges and streamers that dominate in the dusk and pre-midnight sectors. Omega bands have been reported to have an intensity of ~2 $\mu A/m^2$ in the up- and downward currents (Liu et al., 2018), and PAs have a downward (upward) current in the range of ~1–6 (1–3) $\mu A/m^2$ (Gillies et al., 2015). In contrast, auroral streamers are associated with FACs of 25 $\mu A/m^2$ (Amm et al., 1999), and the westward traveling surges are with FACs of 30 $\mu A/m^2$ (Marklund et al., 1998).

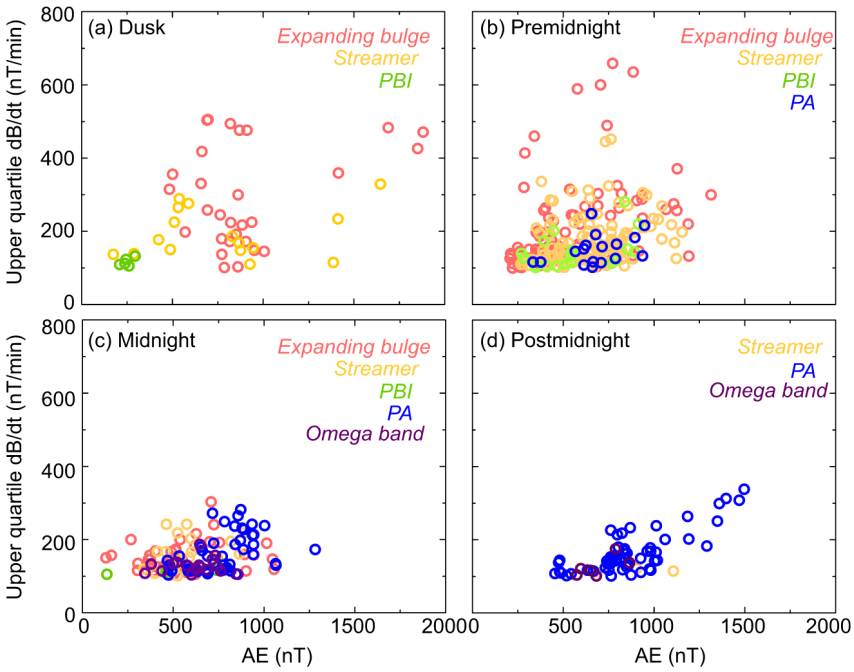

Figure 8. Dependence of the upper quartile of large dB/dt intervals on the type of auroral driver and the AE index. Each open circle represents the upper quartile of one interval. Panels (a–d) represent large dB/dt intervals in the dusk, pre-midnight, midnight, and post-midnight sectors, respectively.

Secondly, dB/dt of very large magnitude (upper quartile >300 nT/min) is primarily driven by the auroral bulges in the dusk and pre-midnight sectors, and to a lesser degree by the streamers. PBI-driven dB/dt is mostly limited to <300 nT/min. Because we define PBIs as non-equatorward extending intensifications, the result implies that more strongly depleted flux tubes have the potential to drive larger dB/dt. Thirdly, dB/dt only shows weak dependence on the AE index with large scatter. The dependence in the dusk and post-midnight sectors is comparatively more prominent than that in the pre-midnight and midnight sectors.

Figure 9 presents the peak value of large dB/dt as a function of the AE index driven by different auroras. The features mentioned above based on the upper quartile also apply to the peak values, with small differences in the midnight sector. In Figure 9c, dB/dt driven by expanding auroral bulges and streamers extend to higher values (600 nT/min) than that with pulsating auroras or omega bands, whereas in Figure 8c, the range of dB/dt is similar. The discrepancy is probably because the very large dB/dt driven by the expanding auroral bulges and streamers in this local time sector only lasts a short amount of time and hence is not captured in the upper quartile but only in the peak values.

5. Discussion

The similarity in the spatiotemporal characteristics between large dB/dt and auroras has important applications because we can now infer the characteristic spatial scale of dB/dt activity by referring to the scale of auroras when the sky is clear. Unlike magnetometers, auroral observations are continuous in space and can even extend beyond continents to achieve a global coverage (with the help of space imaging). Furthermore, when determining the optimum and/or recommended spacing between magnetometer stations that are deployed in arrays to provide continuous monitoring of geomagnetic disturbances for geoelectric fields, we can examine the occurrence, type, and spatial-temporal characteristics of the auroral forms that occur over the area of interest. Auroral bulges typically initiate from a localized brightening along the break-up arc at 21–24 hr MLT and 64°–69° MLAT. Their size depends on the time elapsed from the onset and the azimuthal distance to the onset, and typically reach 5 hr in MLT and 10° in MLAT at its peak (Gjerloev et al., 2007; Mende et al., 2003). Auroral arcs can extend thousands of km long and are usually 18 ± 9 km wide (Knudsen et al., 2001). The associated convection channels bonded by the upward and downward FACs have been reported to be 75 km (Gallardo-Lacourt et al., 2014) and 140–150 km

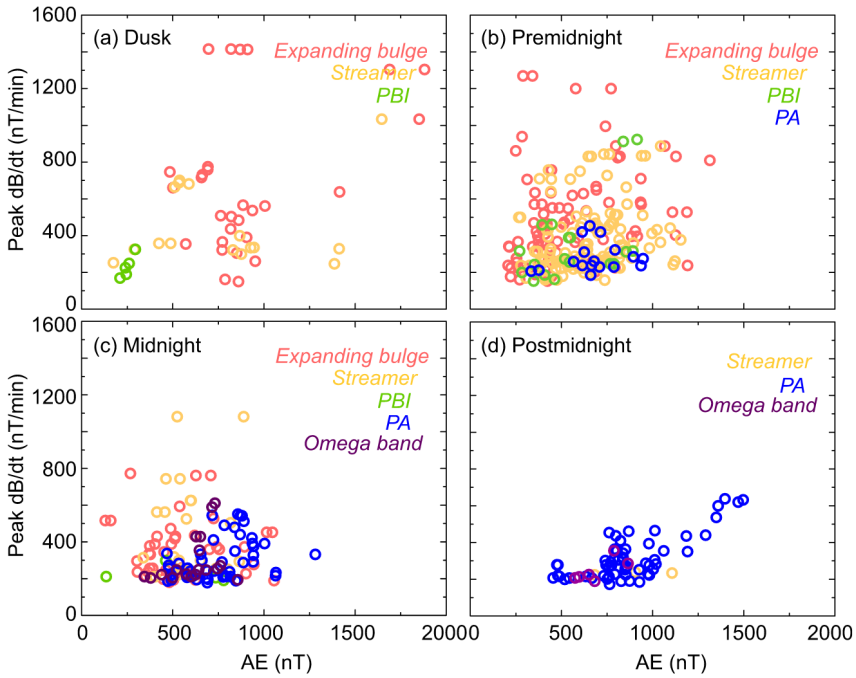

Figure 9. Similar to Figure 8 but showing the peak (defined as the 98 percentile) of large dB/dt intervals.

wide (Gabrielse et al., 2018). Therefore, dB/dt driven by the bulges may simultaneously affect areas over several hundred up to one thousand km, and those driven by auroral arcs can extend thousands of km along the arc but vary drastically in the direction normal to the arcs within 100–200 km. The specific orientation of the arc depends on the local magnetic time and IMF driving.

Similarly, the challenge in determining the onset and duration of dB/dt activity can also be alleviated. Real-time auroral observations, when available, can serve as an advance warning of a potential GIC hazard. In the early expansion phase, the bulge expands at 1.44 and 1.30 km/s in the west and east direction, and 0.66 km/s in the poleward direction. In the late expansion phase, the speed slows down to 0.44 and 0.64 km/s in the west and east direction, and 0.26 km/s in the poleward direction (Gjerloev et al., 2007). Bulges typically last 10–40 min. Streamers often propagate equatorward at a speed of 0.2–0.6 km/s (Gabrielse et al., 2018; Gallardo-Lacourt et al., 2014), and are optical signatures of tail flow bursts organized over 10 min time intervals (Angelopoulos et al., 1992). Omega bands propagate at 0.3–2 km/s, and while the activity can persist continuously for several hours, each bump/torch/tongue structure may take a few to a few tens of min to pass a given magnetometer. The numbers above were obtained manually by scientists, and can further be improved by recent application of machine learning to auroral images which makes an automatic identification and tracking of various auroral forms possible (for example, Clausen & Nickisch, 2018; Kvammen et al., 2020; Nanjo et al., 2022).

One limitation is that the forecast lead time offered by real-time auroras is rather limited, varying from a few to a few tens of minutes.For a longer lead time, we can potentially take advantage of auroral forecast models and adopt their relevant parameterization and modules into the forecasts of GICs. However, existing auroral forecast models, such as the oval variation, assessment, tracking, intensity, and online nowcasting (OVATION Prime) model (Newell, Lee, et al., 2010; Newell, Sotirelis, et al., 2010; Newell, Sotirelis, & Wing, 2010), output the distribution of the large-scale auroral oval with limited information about the embedded auroral forms, yet the latter is important for forecasting the spatially localized and temporally transient large dB/dt events. Nevertheless, progress have been made on capturing and forecasting smaller-scale auroral structures by using both physics-based numerical models (Sorathia et al., 2020) and machine-learning models (McGranaghan et al., 2021), which may potentially contribute to GIC forecast in the future.

Last but not least, by referring to the magnetospheric source of the auroras, the magnetospheric source of dB/dt can be inferred. For example, dB/dt driven by bulges are generated by a tailward and azimuthal expansion of the dipolarized region in the inner magnetosphere that is formed in association with flow bursts transporting

magnetic flux from the reconnection site to the near-Earth region. Those driven by streamers and PBIs are produced by the earthward-moving low-entropy flow bursts. dB/dt driven by omega bands are triggered by flow shears formed either between flows in the plasma sheet and the low-latitude boundary layer or by flow bursts injected into the inner magnetosphere. dB/dt driven by pulsating auroras are caused by interactions between plasma sheet electrons and whistler or ECH waves. This knowledge of the magnetospheric source allows us to better assess the strengths and limitations of existing physical-based models in forecasting dB/dt, and to strategically improve the model performance in the targeted aspects (plasma transportation, instability, wave-particle interaction, etc). For example, when modeling real-event dB/dt with operational numerical models such as the Space Weather Modeling Framework (SWMF (Tóth et al., 2005, 2012)), we can assess the underlying reasons of the false positive and false negative model predictions by referring to auroral observations made at those regions. This is because auroras will reveal what magnetospheric processes are missing, or should not have occurred, in the model. Even for the true positive predictions, auroras will tell whether the model has accurately captured the magnetospheric driver of dB/dt.

6. Summary

Using coordinated observations from THEMIS and GIMA ground magnetometers and THEMIS all-sky imagers, we statistically examine auroral drivers of large dB/dt during geomagnetic storms. A variety of auroral drivers have been identified, including poleward expanding auroral bulges, auroral streamers, PBIs, omega bands, pulsating auroras, etc. The onset, spatial variability, and duration of large dB/dt are well explained by those of the auroras. For example, poleward expanding auroral bulges drive large dB/dt that spread progressively poleward, and periodic injections of streamers drive large dB/dt that occur in periodic bursts. PBIs produce large dB/dt that are confined to the poleward boundary of the auroral oval, and omega bands produce large dB/dt that drift eastward. Pulsating auroras drive large dB/dt that exhibit high-frequency (seconds) fluctuations which could not be captured by data of low cadence such as 1 min.

Statistically, expanding auroral bulges and streamers are dominant drivers in the dusk and pre-midnight sectors, and omega bands and pulsating auroras dominate in the post-midnight sectors. In the midnight sector, large dB/dt can be driven by a wide variety of auroras. The bulge and streamer related dB/dt tends to span a larger range, and therefore can reach higher values, in the dusk and pre-midnight sectors than the dB/dt driven by the omega bands and pulsating auroras in the midnight and post-midnight sectors.

The similarity in the spatiotemporal characteristics between large dB/dt and auroras has important applications because the challenge in determining the spatial variability, onset, and duration of dB/dt activity can be alleviated by referring to auroras. The magnetospheric source of dB/dt can also be inferred. Our results therefore suggest that auroras can exert significant leverage on GIC research and forecast.

Acknowledgments
This work was supported by NASA 80NSSC20K1818. LL and JL are supported by Air Force grant AFOSR FA9559-16-1-0364, NSF grant AGS-2055192, and NASA grants 80NSSC20K1314, 80NSSC20K1316, 80NSSC21K1407, and 80NSSC22K0751, and 80NSSC22K0749. We acknowledge NASA contract NAS5-02099 and V. Angelopoulos for use of data from the THEMIS Mission, specifically S. Mende and E. Donovan for use of the ASI data, the CSA for logistical support in fielding and data retrieval from the GBO stations, and NSF for support of GIMNAST through grant AGS-1004736. We also acknowledge data provided by the Geophysical Institute Magnetometer Array operated by the Geophysical Institute, University of Alaska.

Data Availability Statement

Both the magnetometer and ASI data are available from http://themis.ssl.berkeley.edu/data/themis/thg/.

References

Aikio, A. T., Lakkala, T., Kozlovsky, A., & Williams, P. J. S. (2002). Electric fields and currents of stable drifting auroral arcs in the evening sector. *Journal of Geophysical Research*, *107*(A12), 1424. https://doi.org/10.1029/2001JA009172

Akasofu, S. I., & Kimball, D. S. (1964). The dynamics of the aurora-I. *Journal of Atmospheric and Terrestrial Physics*, *26*(2), 205–211. https://doi.org/10.1016/0021-9169(64)90147-3

Amm, O., Pajunpää, A., & Brandström, U. (1999). Spatial distribution of conductances and currents associated with a north-south auroral form during a multiple-substorm period. *Annals of Geophysics*, *17*(11), 1385–1396. https://doi.org/10.1007/s00585-999-1385-6

Angelopoulos, V., Baumjohann, W., Kennel, C. F., Coroniti, F. V., Kivelson, M. G., Pellat, R., et al. (1992). Bursty bulk flows in the inner central plasma sheet. *Journal of Geophysical Research*, *97*(A4), 4027–4039. https://doi.org/10.1029/91JA02701

Apatenkov, S. V., Pilipenko, V. A., Gordeev, E. I., Viljanen, A., Juusola, L., Belakhovsky, V. B., et al. (2020). Auroral omega bands are a significant cause of large geomagnetically induced currents. *Geophysical Research Letters*, *47*(6). https://doi.org/10.1029/2019GL086677

Belakhovsky, V., Pilipenko, V., Engebretson, M., Sakharov, Y., & Selivanov, V. (2019). Impulsive disturbances of the geomagnetic field as a cause of induced currents of electric power lines. *Journal of Space Weather and Space Climate*, *9*, A18. https://doi.org/10.1051/swsc/2019015

Belakhovsky, V. B., Pilipenko, V. A., Sakharov, Y. a. A., Lorentzen, D. L., & Samsonov, S. N. (2017). Geomagnetic and ionospheric response to the interplanetary shock on 24 January, 2012. *Earth Planets and Space*, *69*(1), 105. https://doi.org/10.1186/s40623-017-0696-1

Campbell, W. H. (1970). Rapid auroral luminosity fluctuations and geomagnetic field pulsations. *Journal of Geophysical Research*, *75*(31), 6182–6208. https://doi.org/10.1029/JA075i031p06182

Campbell, W. H., & Rees, M. H. (1961). A study of auroral coruscations. *Journal of Geophysical Research*, *66*(1), 41–55. https://doi.org/10.1029/JZ066i001p00041

Carter, B. A., Yizengaw, E., Pradipta, R., Weygand, J. M., Piersanti, M., Pulkkinen, A., et al. (2016). Geomagnetically induced currents around the world during the 17 March 2015 storm. *Journal of Geophysical Research: Space Physics*, *121*(10), 10496–10507. https://doi.org/10.1002/2016JA023344

Clausen, L. B., & Nickisch, H. (2018). Automatic classification of auroral images from the Oslo auroral THEMIS (OATH) data set using machine learning. *Journal of Geophysical Research: Space Physics*, *123*(7), 5640–5647. https://doi.org/10.1029/2018ja025274

Connors, M., & Rostoker, G. (1993). Source mechanisms for morning auroral features. *Geophysical Research Letters*, *20*(15), 1535–1538. https://doi.org/10.1029/93GL01594

Dimitrakoudis, S., Milling, D. K., Kale, A., & Mann, I. R. (2022). Sensitivity of ground magnetometer array elements for GIC applications I: Resolving spatial scales with the BEAR and CARISMA arrays. *Space Weather*, *20*(1), e2021SW002919. https://doi.org/10.1029/2021SW002919

Dimmock, A. P., Rosenqvist, L., Hall, J.-O., Viljanen, A., Yordanova, E., Honkonen, I., et al. (2019). The GIC and geomagnetic response over fennoscandia to the 7–8 September 2017 geomagnetic storm. *Space Weather*, *17*(7), 989–1010. https://doi.org/10.1029/2018SW002132

Dimmock, A. P., Rosenqvist, L., Welling, D. T., Viljanen, A., Honkonen, I., Boynton, R. J., & Yordanova, E. (2020). On the regional variability of dB/dt and its significance to GIC. *Space Weather*, *18*(8), e2020SW002497. https://doi.org/10.1029/2020SW002497

Engebretson, M. J., Kirkevold, K. R., Steinmetz, E. S., Pilipenko, V. A., Moldwin, M. B., McCuen, B. A., et al. (2020). Interhemispheric comparisons of large nighttime magnetic perturbation events relevant to GICs. *Journal of Geophysical Research: Space Physics*, *125*(8), e2020JA028128. https://doi.org/10.1029/2020JA028128

Engebretson, M. J., Steinmetz, E. S., Posch, J. L., Pilipenko, V. A., Moldwin, M. B., Connors, M. G., et al. (2019b). Nighttime magnetic perturbation events observed in Arctic Canada: 2. Multiple-instrument observations. *Journal of Geophysical Research: Space Physics*, *124*(9), 7459–7476. https://doi.org/10.1029/2019JA026797

Engebretson, M. J., Pilipenko, V. A., Ahmed, L. Y., Posch, J. L., Steinmetz, E. S., Moldwin, M. B., et al. (2019b). Nighttime magnetic perturbation events observed in Arctic Canada: 1. Survey and statistical analysis. *Journal of Geophysical Research: Space Physics*, *124*, 7442–7458. https://doi.org/10.1029/2019JA026794

Ferdousi, B., Raeder, J., Zesta, E., Cramer, W., & Murphy, K. (2021). Association of auroral streamers and bursty bulk flows during different states of the magnetotail: A case study. *Journal of Geophysical Research: Space Physics*, *126*(9), e2021JA029329. https://doi.org/10.1029/2021JA029329

Fiori, R. a. D., Boteler, D. H., & Gillies, D. M. (2014). Assessment of GIC risk due to geomagnetic sudden commencements and identification of the current systems responsible. *Space Weather*, *12*(1), 76–91. https://doi.org/10.1002/2013SW000967

Freeman, M. P., Forsyth, C., & Rae, I. J. (2019). The influence of substorms on extreme rates of change of the surface horizontal magnetic field in the United Kingdom. *Space Weather*, *17*(6), 827–844. https://doi.org/10.1029/2018SW002148

Fujii, R., Oguti, T., & Yamamoto, T. (1985). Relationships between pulsating auroras and field-aligned electric currents. *Memoirs of National Institute of Polar Research*, *36*, 95–103.

Fukizawa, M., Sakanoi, T., Miyoshi, Y., Hosokawa, K., Shiokawa, K., Katoh, Y., et al. (2018). Electrostatic electron cyclotron harmonic waves as a candidate to cause pulsating auroras. *Geophysical Research Letters*, *45*, 12661–12668. https://doi.org/10.1029/2018GL080145

Gabrielse, C., Nishimura, T., Chen, M., Hecht, J. H., Kaeppler, S. R., Gillies, D. M., et al. (2021). Estimating precipitating energy flux, average energy, and hall auroral conductance from THEMIS all-sky-imagers with focus on mesoscales. *Frontiers in Physics*, *9*, 744298. https://doi.org/10.3389/fphy.2021.744298

Gabrielse, C., Nishimura, Y., Lyons, L., Gallardo-Lacourt, B., Deng, Y., & Donovan, E. (2018). Statistical properties of mesoscale plasma flows in the nightside high-latitude ionosphere. *Journal of Geophysical Research: Space Physics*, *123*(8), 6798–6820. https://doi.org/10.1029/2018JA025440

Gallardo-Lacourt, B., Nishimura, Y., Lyons, L. R., Zou, S., Angelopoulos, V., Donovan, E., et al. (2014). Coordinated SuperDARN THEMIS ASI observations of mesoscale flow bursts associated with auroral streamers. *Journal of Geophysical Research: Space Physics*, *119*(1), 142–150. https://doi.org/10.1002/2013JA019245

Gillies, D. M., Knudsen, D., Spanswick, E., Donovan, E., Burchill, J., & Patrick, M. (2015). Swarm observations of field-aligned currents associated with pulsating auroral patches. *Journal of Geophysical Research: Space Physics*, *120*(11), 9484–9499. https://doi.org/10.1002/2015JA021416

Gjerloev, J. W. (2012). The SuperMAG data processing technique. *Journal of Geophysical Research*, *117*(A9), A09213. https://doi.org/10.1029/2012JA017683

Gjerloev, J. W., Hoffman, R. A., Sigwarth, J. B., & Frank, L. A. (2007). Statistical description of the bulge-type auroral substorm in the far ultraviolet. *Journal of Geophysical Research*, *112*(A7). https://doi.org/10.1029/2006JA012189

Heacock, R. R., & Hunsucker, R. D. (1977). A study of concurrent magnetic field and particle precipitation pulsations, 0.005 to 0.5 Hz, recorded near college. *Journal of Atmospheric and Terrestrial Physics*, *39*(4), 487–501. https://doi.org/10.1016/0021-9169(77)90158-1

Henderson, M. G. (2012). Auroral substorms, poleward boundary activations, auroral streamers, omega bands, and onset precursor activity. In A. Keiling, E. Donovan, F. Bagenal, & T. Karlsson (Eds.), *Auroral phenomenology and magnetospheric processes: Earth and other planets* (pp. 39–54). American Geophysical Union. https://doi.org/10.1029/2011GM001165

Henderson, M. G., Murphree, J. S., & Reeves, G. D. (1994). The activation of the dusk-side and the formation of north-south aligned structures during substorms. *Proceedings of the second international conference on substorms (ICS-2)*, In J. R. Kan, J. D. Craven, & S. Akasofu (Eds.), Geophysical Institute, University of Alaska Fairbanks

Heyns, M. J., Lotz, S. I., & Gaunt, C. T. (2021). Geomagnetic pulsations driving geomagnetically induced currents. *Space Weather*, *19*(2), e2020SW002557. https://doi.org/10.1029/2020SW002557

Hosokawa, K., & Ogawa, Y. (2010). Pedersen current carried by electrons in auroral D-region. *Geophysical Research Letters*, *37*(18), L18103. https://doi.org/10.1029/2010GL044746

Hull, A. J., Wilber, M., Chaston, C. C., Bonnell, J. W., McFadden, J. P., Mozer, F. S., et al. (2010). Time development of field-aligned currents, potential drops, and plasma associated with an auroral poleward boundary intensification. *Journal of Geophysical Research*, *115*(A6), A06211. https://doi.org/10.1029/2009JA014651

Juusola, L., Kauristie, K., van de Kamp, M., Tanskanen, E. I., Mursula, K., Asikainen, T., et al. (2015). Solar wind control of ionospheric equivalent currents and their time derivatives. *Journal of Geophysical Research: Space Physics*, *120*(6), 4971–4992. https://doi.org/10.1002/2015JA021204

Kappenman, J. G. (2005). An overview of the impulsive geomagnetic field disturbances and power grid impacts associated with the violent Sun-Earth connection events of 29–31 October 2003 and a comparative evaluation with other contemporary storms. *Space Weather*, *3*(8). https://doi.org/10.1029/2004SW000128

Kappenman, J. G. (2006). Great geomagnetic storms and extreme impulsive geomagnetic field disturbance events—An analysis of observational evidence including the great storm of May 1921. *Advances in Space Research*, *38*(2), 188–199. https://doi.org/10.1016/j.asr.2005.08.055

Kappenman, J. G., Radasky, W. A., Gilbert, J. L., & Erinmez, L. A. (2000). Advanced geomagnetic storm forecasting: A risk management tool for electric power system operations. *IEEE Transactions on Plasma Science*, *28*(6), 2114–2121. https://doi.org/10.1109/27.902238

Kasahara, S., Miyoshi, Y., Yokota, S., Mitani, T., Kasahara, Y., Matsuda, S., et al. (2018). Pulsating aurora from electron scattering by chorus waves. *Nature*, *554*(7692), 337–340. https://doi.org/10.1038/nature25505

Kepko, L., McPherron, R. L., Amm, O., Apatenkov, S., Baumjohann, W., Birn, J., et al. (2015). Substorm current wedge revisited. *Space Science Reviews*, *190*(1), 1–46. https://doi.org/10.1007/s11214-014-0124-9

Kissinger, J., McPherron, R. L., Hsu, T.-S., & Angelopoulos, V. (2011). Steady magnetospheric convection and stream interfaces: Relationship over a solar cycle. *Journal of Geophysical Research*, *116*(A5), A00I19. https://doi.org/10.1029/2010JA015763

Knudsen, D. J., Donovan, E. F., Cogger, L. L., Jackel, B., & Shaw, W. D. (2001). Width and structure of mesoscale optical auroral arcs. *Geophysical Research Letters*, *28*(4), 705–708. https://doi.org/10.1029/2000gl011969

Kozyreva, O. V., Pilipenko, V. A., Belakhovsky, V. B., & Sakharov, Y. A. (2018). Ground geomagnetic field and GIC response to March 17, 2015, storm. *Earth Planets and Space*, *70*(1), 157. https://doi.org/10.1186/s40623-018-0933-2

Kvammen, A., Wickstrøm, K., McKay, D., & Partamies, N. (2020). Auroral image classification with deep neural networks. *Journal of Geophysical Research: Space Physics*, *125*(10), e2020JA027808. https://doi.org/10.1029/2020ja027808

Lessard, M. R. (2012). *A review of pulsating aurora* (Vol. 55–68). Aurora Phenomenology Magnetospheric Processes Earth Other Planets. https://doi.org/10.1029/2011GM001187

Liu, J., Lyons, L. R., Archer, W. E., Gallardo-Lacourt, B., Nishimura, Y., Zou, Y., et al. (2018). Flow shears at the poleward boundary of omega bands observed during conjunctions of Swarm and THEMIS ASI. *Geophysical Research Letters*, *45*(3), 1218–1227. https://doi.org/10.1002/2017GL076485

Liu, J., Lyons, L. R., Wang, C.-P., Hairston, M. R., Zhang, Y., & Zou, Y. (2020). Dawnside auroral polarization streams. *Journal of Geophysical Research: Space Physics*, *125*(8), e2019JA027742. https://doi.org/10.1029/2019JA027742

Liu, W. W., & Rostoker, G. (1993). On the origin of auroral fingers. *Journal of Geophysical Research*, *98*(A10), 17401–17407. https://doi.org/10.1029/93JA01313

Lyons, L. R., Blanchard, G. T., Samson, J. C., Ruohoniemi, J. M., Greenwald, R. A., Reeves, G. D., & Scudder, J. D. (1998). Near Earth plasma sheet penetration and geomagnetic disturbances. In *New Perspectives on the Earth's Magnetotail*, (Eds) In A. Nishida, S. W. H. Cowley, & D. N. Baker (Eds.), 241. AGU.

Lyons, L. R., Nagai, T., Blanchard, G. T., Samson, J. C., Yamamoto, T., Mukai, T., et al. (1999). Association between GEOTAIL plasma flows and auroral poleward boundary intensifications observed by CANOPUS photometers. *Journal of Geophysical Research*, *104*(A3), 4485–4500. https://doi.org/10.1029/1998ja900140

Marklund, G. T., Karlsson, T., Blomberg, L. G., Lindqvist, P. A., Fälthammar, C. G., Johnson, M. L., et al. (1998). Observations of the electric field fine structure associated with the westward traveling surge and large-scale auroral spirals. *Journal of Geophysical Research*, *103*(A3), 4125–4144. https://doi.org/10.1029/97ja00558

McCuen, B. A., Moldwin, M. B., & Engebretson, M. (2021). Characterization of transient-large-amplitude geomagnetic perturbation events. *Geophysical Research Letters*, *48*(15), e2021GL094076. https://doi.org/10.1029/2021GL094076

McGranaghan, R. M., Ziegler, J., Bloch, T., Hatch, S., Camporeale, E., Lynch, K., et al. (2021). Toward a next generation particle precipitation model: Mesoscale prediction through machine learning (a case study and framework for progress). *Space Weather*, *19*(6), e2020SW002684. https://doi.org/10.1029/2020SW002684

Mende, S. B., Frey, H. U., Morsony, B. J., & Immel, T. J. (2003). Statistical behavior of proton and electron auroras during substorms. *Journal of Geophysical Research*, *108*(A9), 1339. https://doi.org/10.1029/2002ja009751

Mende, S. B., Harris, S. E., Frey, H. U., Angelopoulos, V., Russell, C. T., Donovan, E., et al. (2009). The THEMIS array of ground-based observatories for the study of auroral substorms. In *The THEMIS Mission* (pp. 357–387). Springer.

Molinski, T. (2002). Why utilities respect geomagnetically induced currents. *Journal of Atmospheric and Solar-Terrestrial Physics*, *64*(16), 1765–1778. https://doi.org/10.1016/S1364-6826(02)00126-8

Molinski, T. S., Feero, W. E., & Damsky, B. L. (2000). Shielding grids from solar storms [power system protection]. *IEEE Spectrum*, *37*(11), 55–60. https://doi.org/10.1109/6.880955

Montbriand, L. (1971). The proton aurora and auroral substorm. In B. M. McCormac (Ed.), *The radiating atmosphere* (pp. 366–373). D. Reidel Publishing Company.

Mravlag, E., Scourfield, M. W. J., Walker, A. D. M., Sutcliffe, P. R., & Nielsen, E. (1991). Simultaneous observations of omega band related phenomena in both hemispheres. *Journal of Atmospheric and Terrestrial Physics*, *53*(3–4), 309–317. https://doi.org/10.1016/0021-9169(91)90114-m

Nakamura, R., Baumjohann, W., Scho¨del, R., Brittnacher, M., Sergeev, V. A., Kubyshkina, M., et al. (2001). Earthward flow bursts, auroral streamers, and small expansions. *Journal of Geophysical Research*, *106*(10), 10791–10802. https://doi.org/10.1029/2000ja000306

Nakamura, R., Oguti, T., Yamamoto, T., & Kokubun, S. (1993). Equatorward and poleward expansion of the auroras during auroral substorms. *Journal of Geophysical Research*, *98*(A4), 5743–5759. https://doi.org/10.1029/92JA02230

Nanjo, S., Nozawa, S., Yamamoto, M., Kawabata, T., Johnsen, M. G., Tsuda, T. T., & Hosokawa, K. (2022). An automated auroral detection system using deep learning: Real-time operation in Tromsø, Norway. *Scientific Reports*, *12*(1), 1–12. https://doi.org/10.1038/s41598-022-11686-8

Newell, P. T., Lee, A. R., Liou, K., Ohtani, S.-I., Sotirelis, T., & Wing, S. (2010). Substorm cycle dependence of various types of aurora. *Journal of Geophysical Research*, *115*(A9). https://doi.org/10.1029/2010ja015331

Newell, P. T., Sotirelis, T., Liou, K., Lee, A. R., Wing, S., Green, J., & Redmon, R. (2010). Predictive ability of four auroral precipitation models as evaluated using polar UVI global images. *Space Weather*, *8*(12). https://doi.org/10.1029/2010sw000604

Newell, P. T., Sotirelis, T., & Wing, S. (2010). Seasonal variations in diffuse, monoenergetic, and broadband aurora. *Journal of Geophysical Research*, *115*(A3). https://doi.org/10.1029/2009ja014805

Ngwira, C. M., Pulkkinen, A. A., Bernabeu, E., Eichner, J., Viljanen, A., & Crowley, G. (2015). Characteristics of extreme geoelectric fields and their possible causes: Localized peak enhancements. *Geophysical Research Letters*, *42*(17), 6916–6921. https://doi.org/10.1002/2015GL065061

Ngwira, C. M., Sibeck, D., Silveira, M. V. D., Georgiou, M., Weygand, J. M., Nishimura, Y., & Hampton, D. (2018). A study of intense local dB/dt variations during two geomagnetic storms. *Space Weather*, *16*(6), 676–693. https://doi.org/10.1029/2018SW001911

Nishimura, Y., Bortnik, J., Li, W., Thorne, R. M., Chen, L., Lyons, L. R., et al. (2011). Multievent study of the correlation between pulsating aurora and whistler mode chorus emissions. *Journal of Geophysical Research*, *116*(A11), A11221. https://doi.org/10.1029/2011JA016876

Nishimura, Y., Bortnik, J., Li, W., Thorne, R. M., Lyons, L. R., Angelopoulos, V., et al. (2010). Identifying the driver of pulsating aurora. *Science*, *330*(6000), 81–84. https://doi.org/10.1126/science.1193186

Nishimura, Y., Lyons, L., Zou, S., Angelopoulos, V., & Mende, S. (2010). Substorm triggering by new plasma intrusion: THEMIS all-sky imager observations. *Journal of Geophysical Research*, *115*(A7), A07222. https://doi.org/10.1029/2009JA015166

Oguti, T., & Hayashi, K. (1984). Multiple correlation between auroral and magnetic pulsations: 2. Determination of electric currents and electric fields around a pulsating auroral patch. *Journal of Geophysical Research*, *89*(A9), 7467–7481. https://doi.org/10.1029/JA089iA09p07467

Oguti, T., Meek, J. H., & Hayashi, K. (1984). Multiple correlation between auroral and magnetic pulsations. *Journal of Geophysical Research*, *89*(A4), 2295. https://doi.org/10.1029/JA089iA04p02295

Oliveira, D. M., Arel, D., Raeder, J., Zesta, E., Ngwira, C. M., Carter, B. A., et al. (2018). Geomagnetically induced currents caused by interplanetary shocks with different impact Angles and speeds. *Space Weather*, *16*(6), 636–647. https://doi.org/10.1029/2018SW001880

Opgenoorth, H. J., Oksman, J., Kaila, K. U., Nielsen, E., & Baumjohann, W. (1983). Characteristics of eastward drifting omega bands in the morning sector of the auroral oval. *Journal of Geophysical Research*, *88*(A11), 9171–9185. https://doi.org/10.1029/JA088iA11p09171

Oyedokun, D., Heyns, M., Cilliers, P., & Gaunt, C. T. (2020). Frequency components of geomagnetically induced currents for power system modeling. In *International SAUPEC/RobMech/PRASA Conference, SAUPEC/RobMech/PRASA 2020*. https://doi.org/10.1109/SAUPEC/RobMech/PRASA48453.2020.9041021

Partamies, N., Weygand, J. M., & Juusola, L. (2017). Statistical study of auroral omega bands. *Annales Geophysicae*, *35*(5), 1069–1083. https://doi.org/10.5194/angeo-35-1069-2017

Pulkkinen, A., Bernabeu, E., Eichner, J., Viljanen, A., & Ngwira, C. (2015). Regional-scale high-latitude extreme geoelectric fields pertaining to geomagnetically induced currents. *Earth Planets and Space*, *67*(1), 93. https://doi.org/10.1186/s40623-015-0255-6

Pulkkinen, A., Kuznetsova, M., Ridley, A., Raeder, J., Vapirev, A., Weimer, D., et al. (2011). Geospace environment modeling 2008–2009 challenge: Ground magnetic field perturbations. *Space Weather*, *9*(2). https://doi.org/10.1029/2010sw000600

Pulkkinen, A., Lindahl, S., Viljanen, A., & Pirjola, R. (2005). Geomagnetic storm of 29–31 October 2003: Geomagnetically induced currents and their relation to problems in the Swedish high-voltage power transmission system. *Space Weather*, *3*(8). https://doi.org/10.1029/2004SW000123

Pulkkinen, A., Rastätter, L., Kuznetsova, M., Singer, H., Balch, C., Weimer, D., et al. (2013). Community-wide validation of geospace model ground magnetic field perturbation predictions to support model transition to operations. *Space Weather*, *11*(6), 369–385. https://doi.org/10.1002/swe.20056

Pulkkinen, A., Thomson, A., Clarke, E., & McKay, A. (2003). April 2000 geomagnetic storm: Ionospheric drivers of large geomagnetically induced currents. *Annales Geophysicae*, *21*(3), 709–717. https://doi.org/10.5194/angeo-21-709-2003

Rostoker, G., Lui, A. T. Y., Anger, C. D., & Murphree, J. S. (1987). North-south aligned structures in the midnight sector auroras as viewed by the Viking imager. *Geophysical Research Letters*, *14*(4), 407–410. https://doi.org/10.1029/GL014i004p00407

Rostoker, G., & Samson, J. C. (1984). Can substorm expansive phase effects and low frequency Pc magnetic pulsations be attributed to the same source mechanism? *Geophysical Research Letters*, *11*(3), 271–274. https://doi.org/10.1029/GL011i003p00271

Royrvik, O., & Davis, T. N. (1977). Pulsating aurora: Local and global morphology. *Journal of Geophysical Research*, *82*(29), 4720–4740. https://doi.org/10.1029/JA082i029p04720

Sandahl, I., Sergienko, T., & Brändström, U. (2008). Fine structure of optical aurora. *Journal of Atmospheric and Solar-Terrestrial Physics*, *70*(18), 2275–2292. https://doi.org/10.1016/j.jastp.2008.08.016

Sato, N., Wright, D. M., Carlson, C. W., Ebihara, Y., Sato, M., Saemundsson, T., et al. (2004). Generation region of pulsating aurora obtained simultaneously by the FAST satellite and a Syowa-Iceland conjugate pair of observatories. *Journal of Geophysical Research*, *109*(A10), A10201. https://doi.org/10.1029/2004JA010419

Sato, N., Wright, D. M., Ebihara, Y., Sato, M., Murata, Y., Doi, H., et al. (2002). Direct comparison of pulsating aurora observed simultaneously by the FAST satellite and from the ground at Syowa. *Geophysical Research Letters*, *29*(21), 371–374. https://doi.org/10.1029/2002GL015615

Schillings, A., Palin, L., Opgenoorth, H., Hamrin, M., Rosenqvist, L., Gjerloev, J. W., et al. (2021). *Distribution and occurrence frequency of dB/dt spikes during magnetic storms 1980-2019* (preprint). *Atmospheric Sciences*. https://doi.org/10.1002/essoar.10507354.1

Sergeev, V. A., Sauvaud, J. A., Popescu, D., Kovrazhkin, R. A., Liou, K., Newell, P. T., et al. (2000). Multiple-spacecraft observation of a narrow transient plasma jet in the Earth's plasma sheet. *Geophysical Research Letters*, *27*(6), 851–854. https://doi.org/10.1029/1999gl010729

Sorathia, K. A., Merkin, V. G., Panov, E. V., Zhang, B., Lyon, J. G., Garretson, J., et al. (2020). Ballooning-interchange instability in the near-Earth plasma sheet and auroral beads: Global magnetospheric modeling at the limit of the MHD approximation. *Geophysical Research Letters*, *47*(14), e2020GL088227. https://doi.org/10.1029/2020GL088227

Størmer, C. (1955). *The polar aurora*. Clarendon Press.

Tóth, G., Sokolov, I. V., Gombosi, T. I., Chesney, D. R., Clauer, C. R., Zeeuw, D. L. D., et al. (2005). Space weather modeling framework: A new tool for the space science community. *Journal of Geophysical Research*, *110*(A12), A12226. https://doi.org/10.1029/2005JA011126

Tóth, G., van der Holst, B., Sokolov, I. V., Zeeuw, D. L. D., Gombosi, T. I., Fang, F., et al. (2012). Adaptive numerical algorithms in space weather modeling. *Journal of Computational Physics*, *231*(3), 870–903. https://doi.org/10.1016/j.jcp.2011.02.006

Vakhnina, V. V., Kuvshinov, A. A., Shapovalov, V. A., Chernenko, A. N., & Kretov, D. A. (2015). The development of models for assessment of the geomagnetically induced currents impact on electric power grids during geomagnetic storms. *Advances in Electrical and Computer Engineering*, *15*(1), 49–54. https://doi.org/10.4316/AECE.2015.01007

Viljanen, A. (1997). The relation between geomagnetic variations and their time derivatives and implications for estimation of induction risks. *Geophysical Research Letters*, *24*(6), 631–634. https://doi.org/10.1029/97GL00538

Viljanen, A., Nevanlinna, H., Pajunpää, K., & Pulkkinen, A. (2001). Time derivative of the horizontal geomagnetic field as an activity indicator. *Annales Geophysicae*, *19*(9), 1107–1118. https://doi.org/10.5194/angeo-19-1107-2001

Viljanen, A., & Tanskanen, E. (2011). Climatology of rapid geomagnetic variations at high latitudes over two solar cycles. *Annales Geophysicae*, *29*(10), 1783–1792. https://doi.org/10.5194/angeo-29-1783-2011

Viljanen, A., Tanskanen, E. I., & Pulkkinen, A. (2006). Relation between substorm characteristics and rapid temporal variations of the ground magnetic field. *Annals of Geophysics*, *9*.

Weigel, R. S., Klimas, A. J., & Vassiliadis, D. (2003). Solar wind coupling to and predictability of ground magnetic fields and their time derivatives. *Journal of Geophysical Research*, *108*(A7), 1298. https://doi.org/10.1029/2002JA009627

Weigel, R. S., Vassiliadis, D., & Klimas, A. J. (2002). Coupling of the solar wind to temporal fluctuations in ground magnetic fields. *Geophysical Research Letters*, *29*(19), 211–214. https://doi.org/10.1029/2002GL014740

Weygand, J. M. (2021). The temporal and spatial development of dB/dt for substorms. *AIMS Geosciences*, *7*(1), 74–94. https://doi.org/10.3934/geosci.2021004

Weygand, J. M., El-Alaoui, M., & Nykyri, H. K. (2022). The source of auroral omegas. *Journal of Geophysical Research: Space Physics*, *127*(1), e2021JA029908. https://doi.org/10.1029/2021JA029908

Weygand, J. M., Kivelson, M. G., Frey, H. U., Rodriguez, J. V., Angelopoulos, V., Redmon, R., et al. (2015). An interpretation of spacecraft and ground based observations of multiple omega band events. *Journal of Atmospheric and Solar-Terrestrial Physics*, *133*, 185–204. https://doi.org/10.1016/j.jastp.2015.08.014

Yagova, N. V., Pilipenko, V. A., Sakharov, Y. A., & Selivanov, V. N. (2021). Spatial scale of geomagnetic Pc5/Pi3 pulsations as a factor of their efficiency in generation of geomagnetically induced currents. *Earth Planets and Space*, *73*(1), 88. https://doi.org/10.1186/s40623-021-01407-2

Yamamoto, T. (1988). On the temporal fluctuations of pulsating auroral luminosity. *Journal of Geophysical Research*, *93*(A2), 897. https://doi.org/10.1029/JA093iA02p00897

Yamamoto, T., Makita, K., Ozaki, M., & Meng, C. I. (1993). A particle simulation of auroral omega bands and torch-like structures. *Journal of Geomagnetism and Geoelectricity*, *45*(8), 619–648. https://doi.org/10.5636/jgg.45.619

Zesta, E., Donovan, E., Lyons, L., Enno, G., Murphree, J. S., & Cogger, L. (2002). Two-dimensional structure of auroral poleward boundary intensifications. *Journal of Geophysical Research*, *107*(A11), 1350. https://doi.org/10.1029/2001JA000260

Zesta, E., Lyons, L., Wang, C.-P., Donovan, E., Frey, H., & Nagai, T. (2006). Auroral poleward boundary intensifications (PBIs): Their two-dimensional structure and associated dynamics in the plasma sheet. *Journal of Geophysical Research*, *111*(A5), A05201. https://doi.org/10.1029/2004JA010640

Zhang, J. J., Wang, C., Sun, T. R., Liu, C. M., & Wang, K. R. (2015). GIC due to storm sudden commencement in low-latitude high-voltage power network in China: Observation and simulation. *Space Weather*, *13*(10), 643–655. https://doi.org/10.1002/2015SW001263

Zou, S., Lyons, L. R., & Nishimura, Y. (2012). Mutual evolution of aurora and ionospheric electrodynamic features near the Harang reversal during substorms. In A. Keiling, E. Donovan, F. Bagenal, & T. Karlsson (Eds.), *Auroral Phenomenology and Magnetospheric Processes: Earth and other Planets*. https://doi.org/10.1029/2011GM001163